Kramers' Diffusion Theory Applied to Gating Kinetics of Voltage-Dependent Ion Channels

Daniel Sigg,* Hong Qian,# and Francisco Bezanilla*
*Department of Physiology and Department of Anesthesiology, School of Medicine, University of California, Los Angeles, California 90095, and #Department of Applied Mathematics, University of Washington, Seattle, Washington 98195 USA

ABSTRACT Kramers' diffusion theory of reaction rates in the condensed phase is considered as an alternative to the traditional discrete-state Markov (DSM) model in describing ion channel gating current kinetics. Diffusion theory can be expected to be particularly relevant in describing high-frequency (>100 kHz) events in channel activation. The generalized voltage sensor of a voltage-dependent ion channel is treated as a Brownian motion particle undergoing spatial diffusion along a one-dimensional energy landscape. Two classes of energy landscapes are considered. The first class contains large barriers, which give rise to gating currents with two distinct time scales: the usual low-frequency decay, which can modeled with a DSM scheme, and a high-frequency component arising from intrastate relaxation. Large depolarizations reduce potential barriers to such a degree that activation rates are diffusion limited, causing the two time scales to merge. Landscapes of the second class are either featureless or contain barriers that are small compared to kT; these are termed "drift landscapes." These landscapes require a larger friction coefficient to generate slow gating kinetics. The high-frequency component that appears with barrier models is not present in pure drift motion. The presence of a high-frequency component can be tested experimentally with large-bandwidth recordings of gating currents. Topics such as frequency domain analysis, spatial dependence of the friction coefficient, methods for determining the adequacy of a DSM model, and the development of physical models of gating are explored.

INTRODUCTION

There is little doubt that conformational changes in ion channels responsible for the generation of action potentials in nerve and muscle are regulated through interactions between "gating" charges and the membrane potential. However, primarily because of the lack of high-resolution structures of voltage-dependent channel proteins, progress in the understanding of ion channel function from a physical standpoint has been frustratingly slow. On the other hand, 50 years of voltage-clamp data from ion channels have produced a wealth of kinetic detail on the physiologic time scale that is unparalleled in the study of slow protein dynamics. The need to describe and catalog this vast data set has led to empirical models in which gating consists of charge translocation between a finite number of discrete Markovian states. These discrete-state Markov (DSM) models, which traditionally utilize Eyring's absolute rate theory, have been very successful in reproducing the time course of electrophysiologic events, but they currently lack a physical interpretation that is consistent with the perceived properties of large proteins. In this communication, we propose an alternative model of ion channel gating based on diffusion, much of which is embodied in Kramers' theory of activated processes in the condensed phase (Kramers, 1940). The reasons for doing so are threefold: (1) Kramers' theory acknowledges the effect of frictional forces on dynamics, a crucial step in developing a realistic physical model of gating; (2) the physiologically relevant slow time behavior of gating in the diffusion theory is similar to that predicted by traditional DSM models, providing a common ground for the two approaches; (3) diffusion theory can be extended to a faster time scale than that of activated events, leading to an explanation of recent voltage-clamp relaxation experiments in which early fast components ($\sim\mu$s) were observed in ion channel gating currents (Forster and Greeff, 1992; Stefani and Bezanilla, 1996).

Friction plays an important role in the kinetics of any large system in which there is strong coupling between macroscopic mechanical variables and numerous, rapidly fluctuating, internal degrees of freedom. Given the size of ion channels and their interactions with a solvent/lipid environment, it is not unreasonable to suppose that any large-scale conformational process such as channel activation must involve friction damping. As a consequence of the fluctuation-dissipation theorem, mechanical variables experiencing strong friction retardation tend to fluctuate in a diffusive manner known as Brownian motion. The most relevant mechanical variable in describing voltage dependence in ion channels is the overall electric dipole moment of the protein/solvent system, a measurable quantity whose mean value for a given temperature and pressure is determined by the applied membrane potential. Because of the manner in which the system dipole moment is measured (through distant electrodes immersed in a conducting bath), it is often referred to as the gating charge displacement, q, and assigned units of charge.

Received for publication 9 December 1997 and in final form 6 October 1998.

Address reprint requests to Dr. Francisco Bezanilla, Department of Physiology, University of California–Los Angeles, 10833 Le Conte Ave., Los Angeles, CA 90095. Tel.: 310-825-2735; Fax: 310-794-9612; E-mail: fbezanil@ucla.edu.

0006-3495/99/02/782/22 $2.00

The main premise of this paper states that the activation kinetics of a voltage-dependent channel are equivalent to the Brownian motion of a gating particle diffusing across an n-dimensional energy landscape. The energy landscape is ideally obtained from structural knowledge of the voltage gating mechanism. For now, we utilize a phenomenologic approach in which we assume that the value of q is a reliable measure of the progress of activation (referred to hereafter as the position of a fictitious gating particle) and require that the energy landscape be a one-dimensional potential of mean force (pmf) with respect to q. The equation describing overdamped diffusive motion in a one-dimensional pmf is attributed to Smoluchowski and was used by Kramers to develop his theory of activated transition rates in the limit of large friction. The Smoluchowski equation may be written in the form

$$\frac{\delta}{\delta t}p = -\frac{\delta}{\delta q}\left[\frac{-W'(q)}{R(q)}p - \frac{kT}{R(q)}\frac{\delta}{\delta q}p\right] \qquad (1)$$

where $p(q, t)$ is the probability density of the gating particle at position q and time t, $W(q)$ is the pmf, $R(q)$ is the friction coefficient, k is Boltzmann's constant, and T is the absolute temperature. The Smoluchowski equation is essentially a statement of local probability conservation in which two types of condensed phase motions, drift and diffusion, are featured inside the brackets as the first and second terms. Drift motion occurs in the presence of a pmf gradient, producing a directed displacement of the probability distribution to a region of local energy minima. Diffusive motion broadens the probability distribution in both directions and allows activated transitions over energy barriers to take place. In thermal equilibrium, the tendencies of drift and diffusion balance each other, and the equilibrium probability distribution is found through the Boltzmann distribution, $p(q, \infty) = C \exp(-W(q)/kT)$.

We extend Kramers' treatment slightly by allowing the friction coefficient R to be position dependent. According to Van Kampen (1992), this leads to some ambiguity in the choice of diffusion equations. Equation 1 has the advantage of satisfying the canonical Boltzmann distribution at thermal equilibrium, so it is our natural choice. However, it has the curious feature of producing a transient flux along a friction gradient in the absence of a pmf gradient, a phenomenon known as "spurious drift." As we shall see, spatial variation of the friction coefficient plays a potentially important role in generating nonstationary gating current fluctuations in drift diffusion models.

Given the success of the DSM model in modeling gating kinetics, it is worth knowing the circumstances under which a diffusion model can be represented by a DSM model. Clearly, well-defined states occur only through local minima in the energy landscape, and to satisfy the Markovian property of exponential dwell times, activation barriers must be sufficiently high in energy. How high? The criteria may be found in calculating time-dependent rates over the barrier, and will be investigated in the Results. On the "slow" physiologic time scale (defined by typical dwell times within states), large barrier diffusion models predict kinetics identical to those of DSM models. Barrier transitions with concomitant charge displacement generate bandwidth limited spikes in the single-channel gating current. Although individual transition spikes are too small to be measured experimentally, records from a large ensemble of channels can detect fluctuations in the gating current, which have the characteristics of shot noise (Rice, 1944; Conti and Stühmer, 1989; Crouzy and Sigworth, 1993; Sigg et al., 1994).

There are clearly instances where a continuum state description is necessary. DSM models fail to describe events on a "fast" time scale, such as relaxation within a metastable state or the exact trajectory taken by the gating particle as it crosses the activated region. In the presence of a pmf gradient, the mean gating current over very brief time spans is often given by the drift velocity, $i = -W'(q)/R$. Experimentally, one method with which to record drift events is the use of large bandwidth recordings of the initial current transient after a rapid voltage step. In such an experiment, the early component of the gating current can be thought of as the rapid settling of the gating particle to a new equilibrium position in the depths of a metastable state. Evidence for the existence of an early fast component of gating comes from recent recordings by Stefani and Bezanilla (1996) of gating currents obtained in giant patch recordings of *Shaker* potassium channels. They measured ~5-μs current transients that decayed two orders of magnitude more rapidly than the fastest of the typical slow gating components. Similar events have been recorded using sodium channels (Forster and Greeff, 1992). A second method of recording drift currents is the application of extreme membrane potentials, thereby obliterating energy barriers. This leads to drift-limited activation, the rate of which deviates significantly from the exponential voltage dependence predicted by the Arrhenius-type rate constants used in DSM models.

It is possible to imagine a pmf landscape devoid of large barriers, which will be referred to as a "drift landscape." In a drift landscape, there are no activated transition events, and the gating current is equal to the drift velocity of the gating particle. Drift landscapes require large friction coefficients to prevent rapid traversal of the gating particle along the activation path. Whereas barrier models generate shot noise in the range of physiological frequencies, gating current fluctuations from drift processes have the same spectral characteristics as those of Nyquist (Johnson) noise measured across the terminals of a resistor (this is also true for barrier models at very high frequencies). Implicitly or explicitly, drift landscapes have been considered by several investigators (Millhauser et al., 1988; Läuger, 1988; Levitt, 1989; Condat and Jäckle, 1989) as the basis for ion channel gating. As we will see later, drift processes with constant friction probably do not describe the gating of many channels, as they fail to predict two features that have been observed experimentally in voltage-sensitive sodium and potassium channels: the brief duration of the early compo-

nent of the gating current (Stefani and Bezanilla, 1996; Forster and Greeff, 1992) and nonstationary gating current fluctuations (Conti and Stühmer, 1989; Crouzy and Sigworth, 1993; Sigg et al., 1994). Nevertheless, as will be demonstrated in the Results, nonstationary variance is made possible in a drift model by allowing the friction coefficient to have spatial dependence.

A primary issue that will be addressed in this communication is one of practicality: can the techniques developed here be easily implemented to improve our present understanding of ion channel kinetics? A physical theory, no matter how elegant, is worth little in the long run if it is not easily related to experimental results. The challenge in employing a continuum description of the channel is the computational workload required to predict kinetics for an arbitrarily shaped landscape. Fortunately, computer technology has progressed to the point where complex numerical problems can be solved in a relatively short time. A strength of the DSM approach is its flexibility and ease of application. It was our aim to achieve a similar level of "user friendliness" with the proposed diffusion theory. This was achieved mainly through a master equation description of the model system dynamics, which allowed us to use standard methods to reduce the system to distinct eigencomponents. With the addition of some refinements to improve speed and enable slow sampling of fast eigencomponents, many of the computations could be performed rapidly enough to be used as a part of a fitting routine for data analysis.

THEORY

Numerical analysis of gating kinetics

To numerically predict the response of a model channel to a depolarizing pulse, we cast the system of coupled differential equations describing the kinetics of the model into a master equation known as a "Q-matrix" (Colquhoun and Hawkes, 1995). A master equation provides an exact stochastic description of a DSM model, and continuum models may be approximated by a discrete master equation with a suitable discretization scheme. The use of a master equation in predicting gating currents and their fluctuations in DSM models has already been described (Frehland, 1978; Crouzy and Sigworth, 1993). The extension of the procedure to continuum models requires adjustments in application that increase the efficiency of numerical computation and allow undersampling of high-frequency events.

The master equation is a statement of probability flux between Markovian (memoryless) states of a system (Papoulis, 1991). In a closed system such as the gating apparatus of a channel, total probability is conserved, and the rate of probability redistribution is determined by the set of transition rate constants a_{ij}. A compact formulation of the master equation is given by

$$\frac{\mathrm{d}}{\mathrm{d}t}\mathbf{P}(t) = \mathbf{P}(t)\mathbf{A} \tag{2}$$

where the elements of the $n \times n$ matrix $\mathbf{P}$ are the transition probabilities $\{p_{ij}(t)\} = p(j, t|i, 0)$, and $\mathbf{A}$ is given by $\{a_{ij} - \Sigma_k a_{ik}\delta_{ij}\}$. We have written the master equation in row-major (Q-matrix) form, contrary to usage by some authors (Van Kampen, 1992; Frehland, 1978). In row-major form, the element a_{ij} signifies a transition from i to j, rather than from j to i, as it would be written in column-major notation.

The solution to the master equation is

$$\mathbf{P}(t) = \exp(\mathbf{A}t) \tag{3}$$

The state probability vector $\mathbf{p}(t)$ is obtained from initial conditions $\mathbf{p}(t_o)$ through the Kolmogorov equation,

$$\langle\mathbf{p}(t)| = \langle\mathbf{p}(t_o)|\mathbf{P}(t - t_o) \tag{4}$$

where Dirac's bracket notation is used to denote row ($\langle\mathbf{v}|$) and column ($|\mathbf{v}\rangle$) vectors. A rapid method for obtaining the time-dependent moments of the gating charge displacement is eigenvalue decomposition of **A.** Diagonalization of **A** is simplified by constructing the symmetric matrix $\mathbf{A}_s$ through the following operation (Frehland, 1978):

$$\mathbf{A}_s = \mathbf{P}_e^{1/2}\mathbf{A}\mathbf{P}_e^{-1/2} \tag{5}$$

where $\mathbf{P}_e = \{p_i(\infty)\delta_{ij}\}$ is a diagonal matrix whose elements are the state probabilities during thermal equilibrium. The eigenvalues λ_r and corresponding eigenvectors Ψ_r of $\mathbf{A}_s$ are obtained in a straightforward manner by numerical routines specialized for symmetric matrices (Press et al., 1992). Back-transformation to the eigencomponents of **A** is achieved through the relations

$$\begin{aligned}\langle\mathbf{u}_r| &= \langle\Psi_r|\mathbf{P}_e^{1/2}\\ |\mathbf{v}_r\rangle &= \mathbf{P}_e^{-1/2}|\Psi_r\rangle\end{aligned} \tag{6}$$

where $\mathbf{u}_r$ and $\mathbf{v}_r$ are the left and right eigenvectors, respectively. The eigenvalues λ_r are invariant under transformation. With initial distribution of states $\mathbf{p}_o = \mathbf{p}(0)$, the ensemble mean and autocorrelation of the displacement are

$$\begin{aligned}\langle q(t)\rangle &= \langle\mathbf{p}_o|\mathbf{P}(t)|\mathbf{q}\rangle\\ &= \sum_r \rho_r \exp(\lambda_r t)\end{aligned} \tag{7a}$$

$$\begin{aligned}\langle q(t_1)q(t_2 \geq t_1)\rangle &= \langle\mathbf{p}_o|\mathbf{P}(t_1)\mathbf{Q}\mathbf{P}(t_2 - t_1)|\mathbf{q}\rangle\\ &= \sum_{r,s} \eta_{rs}\exp(\lambda_r t_1)\exp(\lambda_s(t_2 - t_1))\end{aligned} \tag{7b}$$

where $\mathbf{q} = \{q_i\}$ contains the state positions, and the diagonal matrix $\mathbf{Q} = \{q_i\delta_{ij}\}$. The weighing terms ρ and η are given by

$$\begin{aligned}\rho_r &= \langle\mathbf{p}_o|\mathbf{v}_r\rangle\langle\mathbf{u}_r|\mathbf{q}\rangle\\ \eta_{rs} &= \langle\mathbf{p}_o|\mathbf{v}_r\rangle\langle\mathbf{u}_r|\mathbf{Q}|\mathbf{v}_s\rangle\langle\mathbf{u}_s|\mathbf{q}\rangle\end{aligned} \tag{8}$$

Evaluation of any of the brackets in Eq. 8 requires only a single summation over n states, which is speedily done with modern computers. Although the autocorrelation given by

Eq. 7b is specified only for times $t_2 \geq t_1$, the complete matrix is easily obtained from the fact that the autocorrelation function is diagonally symmetric around $t_1 = t_2$.

To find the moments of the gating current, $i = \mathrm{d}q/\mathrm{d}t$, namely the mean, $\mu(t) = \langle i(t) \rangle$, and autocorrelation, $\mathrm{corr}(t_1, t_2) = \langle i(t_1) i(t_2) \rangle$, we differentiate Eqs. 7a,b (Papoulis, 1991):

$$\mu(t) = \frac{\mathrm{d}}{\mathrm{d}t} \langle q(t) \rangle \tag{9a}$$

$$\mathrm{corr}(t_1, t_2) = \frac{\partial^2}{\partial t_1 \partial t_2} \langle q(t_1) q(t_2) \rangle \tag{9b}$$

Taking into consideration the discontinuity in the partial derivative of the autocorrelation function at $t_1 = t_2$, the final result is

$$\mu(t) = \sum_{\mathrm{r}} \omega_{\mathrm{r}} \exp(\lambda_{\mathrm{r}} t) \tag{10a}$$

$$\mathrm{corr}(t_1, t_2 \geq t_1) = \sum_{\mathrm{r}} \chi_{\mathrm{r}} \exp(\lambda_{\mathrm{r}} t_1) \delta(t_2 - t_1) \tag{10b}$$

$$+ \sum_{\mathrm{r,s}} \upsilon_{\mathrm{rs}} \exp(\lambda_{\mathrm{r}} t_1) \exp(\lambda_{\mathrm{s}} (t_2 - t_1)) \tag{10c}$$

The gating current weighing terms ω, χ, and υ in Eq. 10 are easily computed from their counterparts in the gating charge displacements (Eq. 8):

$$\begin{aligned} \omega_{\mathrm{r}} &= \rho_{\mathrm{r}} \lambda_{\mathrm{r}} \\ \chi_{\mathrm{r}} &= \sum_{\mathrm{s}} \eta_{\mathrm{rs}} (\lambda_{\mathrm{r}} - 2\lambda_{\mathrm{s}}) \\ \upsilon_{\mathrm{rs}} &= \eta_{\mathrm{rs}} (\lambda_{\mathrm{r}} - \lambda_{\mathrm{s}}) \lambda_{\mathrm{s}} \end{aligned} \tag{11}$$

The one-sided power spectrum $S(\omega)$ of the gating current can be computed from the steady-state form of the autocorrelation function (Eq. 10b,c) through application of the Wiener-Khintchine theorem. Written as a function of the angular frequency ω,

$$S(\omega) = 2\chi_{\mathrm{o}} - \sum_{\mathrm{s}} \upsilon_{\mathrm{os}} \frac{4\lambda_{\mathrm{s}}}{\omega^2 + \lambda_{\mathrm{s}}^2} \tag{12}$$

Crouzy and Sigworth (1993) expressed the gating current weighing terms as functions of the rate constants a_{ij} and transition charge movements $q_{\mathrm{ij}} = q_{\mathrm{j}} - q_{\mathrm{i}}$. With some algebraic manipulation, the weights in Eq. 11 are found to be equivalent to theirs, which are given by

$$\begin{aligned} \omega_{\mathrm{r}} &= \langle \mathbf{p}_{\mathrm{o}} | \mathbf{v}_{\mathrm{r}} \rangle \langle \mathbf{u}_{\mathrm{r}} | \Theta_{\mathrm{g}} | \mathbf{1} \rangle \\ \chi_{\mathrm{r}} &= \langle \mathbf{p}_{\mathrm{o}} | \mathbf{v}_{\mathrm{r}} \rangle \langle \mathbf{u}_{\mathrm{r}} | \Theta_{\mathrm{v}} | \mathbf{1} \rangle \\ \upsilon_{\mathrm{rs}} &= \langle \mathbf{p}_{\mathrm{o}} | \mathbf{v}_{\mathrm{r}} \rangle \langle \mathbf{u}_{\mathrm{r}} | \Theta_{\mathrm{g}} | \mathbf{v}_{\mathrm{s}} \rangle \langle \mathbf{u}_{\mathrm{s}} | \mathbf{1} \rangle \end{aligned} \tag{13}$$

where the elements of the moment matrixes, Θ_{g} and Θ_{v}, are $\{a_{\mathrm{ij}} q_{\mathrm{ij}}\}$ and $\{a_{\mathrm{ij}} q_{\mathrm{ij}}^2\}$, respectively.

Although Eq. 13 is less efficient for numerical computation than its counterparts in Eq. 11, expressing weighing factors as a function of the moment matrixes gives a more intuitive interpretation of the equations describing gating currents and their fluctuations. This is illustrated by the concept of the *elementary charge displacement* Δq_{e} in DSM models, defined as (Conti and Stühmer, 1989; Sigg et al., 1994)

$$\Delta q_{\mathrm{e}}(t) \equiv \frac{\mathrm{var}(t)}{2B\mu(t)} \tag{14}$$

where B is the effective bandwidth of the recording apparatus (see Methods). Using moment matrices Θ_{g} and Θ_{v}, an expression for $\Delta q_{\mathrm{e}}(t)$ valid at high bandwidths is given by

$$\Delta q_{\mathrm{e}}(t) \cong \frac{\langle \mathbf{p}(t) | \Theta_{\mathrm{v}} | \mathbf{1} \rangle}{\langle \mathbf{p}(t) | \Theta_{\mathrm{g}} | \mathbf{1} \rangle} = \frac{\sum_{\mathrm{I,J}} p_{\mathrm{I}}(t) k_{\mathrm{IJ}} q_{\mathrm{IJ}}^2}{\sum_{\mathrm{I,J}} p_{\mathrm{I}}(t) k_{\mathrm{IJ}} q_{\mathrm{IJ}}} \tag{15}$$

where B is assumed to be large compared to the individual transition rate constants k_{IJ}, causing the delta term (Eq. 10b, $t_1 = t_2$) to dominate the variance. Assuming that every forward transition occurs with equal probability (a gross simplification), with chances of very few backward transitions (which can be achieved by stepping to sufficiently depolarized voltages), Δq_{e} becomes time independent and has the value (Conti and Stühmer, 1989)

$$\Delta q_{\mathrm{e}} \cong \frac{\sum_{\mathrm{I,J}} q_{\mathrm{IJ}}^2}{\sum_{\mathrm{I,J}} q_{\mathrm{IJ}}} \tag{16}$$

where the sum runs over only positive charge-carrying transitions. According to Eq. 16, Δq_{e} is the self-weighted average of the elementary charge movements. Therefore, if the assumptions leading to Eq. 16 are valid, the experimentally derived value of Δq_{e} gives a rough estimate of the largest charge moved by any one transition in the kinetic sequence.

Discretization of the Smoluchowski equation

The master equation approach (Eq. 2) may be used to describe diffusion in a pmf landscape if the state space is finely discretized. To demonstrate this, we rewrite the Smoluchowski equation (Eq. 1) in the standard Fokker-Planck form,

$$\frac{\partial p}{\partial t} = F\{p\} \tag{17}$$

where F is the spatially continuous Fokker-Planck operator

$$F = -\frac{\delta}{\delta q} A(q) + \frac{1}{2} \frac{\delta^2}{\delta q^2} B(q) \tag{18}$$

and the first and second moments, $A(q)$ and $B(q)$, are given by

$$\begin{aligned} A(q) &= \frac{-U'(q)}{R(q)} \\ B(q) &= \frac{2kT}{R(q)} \end{aligned} \tag{19}$$

The energy term, $U(q)$, is the sum of the pmf $W(q)$ and the "spurious drift" term:

$$U(q) = W(q) + kT \ln R(q) \tag{20}$$

The parallel with the master equation formalism should be clear, and discretizing Eq. 18 into small increments of Δq will transform it into a "Q"-matrix. We employ a linear sequential scheme in which Δq is made as small, which is realistic from a computational standpoint (Fig. 1). To avoid confusion due to the fact that both DSM and diffusion models are represented by a master equation, we assign Greek letters to "rate constants" between incremental steps in the discretized diffusion model and use the letter k for transition rate constants in a DSM model. The n-state diffusion scheme is described by $n - 1$ equations of the form

$$\frac{\mathrm{d}}{\mathrm{d}t}p(i\Delta q) = \alpha_{i-1}p((i-1)\Delta q) + \beta_{i+1}p((i+1)\Delta q) - \alpha_i p(i\Delta q) - \beta_i p(i\Delta q) \tag{21}$$

where $p(q)$ is shorthand for $p(q, t)$. By expanding the probabilities around $p(i\Delta q)$ up to second order in Δq and performing a similar expansion for the rate constants α, β around the values α_i, β_i, respectively, we obtain the Fokker-Planck equation if powers greater than 2 are neglected and the rate constants satisfy

$$\alpha_i = \frac{B(i\Delta q)}{2\Delta q^2}\left(1 + \frac{A(i\Delta q)\Delta q}{B(i\Delta q)}\right) \tag{22a}$$

$$\beta_i = \frac{B(i\Delta q)}{2\Delta q^2}\left(1 - \frac{A(i\Delta q)\Delta q}{B(i\Delta q)}\right) \tag{22b}$$

Although they lead to the correct form in the limit of vanishing Δq, Eq. 22 tends to be inadequate for use in practice, since abrupt changes in the effective energy $W + kT \ln R$ occurring within a single spatial increment lead to a negative value for either the forward or backward rate constant in that region, which is a nonsensical result. Moreover, much care must be given in evaluating the term $A(i\Delta q)\Delta q$. Since $A(q)$ contains a derivative, several interpretations are possible when one begins with discretized state space. Most can be rejected on the basis that the resulting stationary probability distribution fails to satisfy detailed balance.

To circumvent these problems, we make use of the concept of splitting probability, which is the probability of exiting a region at a specific location given an initial starting point. The local potential around position C_i is approximated by the staircase function shown in Fig. 1. Starting from C_i, the forward splitting probability π_a of attaining the position C_{i+1} is

$$\pi_a = \frac{\alpha_i}{\alpha_i + \beta_i} \tag{23}$$

Adding Eq. 22a,b and substituting into Eq. 23, we obtain an expression for α_i that has the form of the forward rate of a random walk:

$$\alpha_i = \frac{2kT}{R_i \Delta q^2}\,\pi_a \tag{24}$$

The splitting probability π_a is found from the following expression (Van Kampen, 1992):

$$\pi_a = \frac{\int_{q_{i-}}^{q_i} R(q)\exp(W(q)/kT)\mathrm{d}q}{\int_{q_{i-1}}^{q_{i+1}} R(q)\exp(W(q)/kT)\mathrm{d}q} \tag{25}$$

Evaluating the integrals for the region between C_{i-1} and C_{i+1} in Fig. 1, we obtain

$$\pi_a = \left[1 + \frac{1 + (R_{i+1}/R_i)\exp((W_{i+1} - W_i)/kT)}{1 + (R_{i-1}/R_i)\exp((W_{i-1} - W_i)/kT)}\right]^{-1} \tag{26}$$

Detailed balance is ensured by computing β_{i+1} using the Boltzmann equation:

$$\frac{\alpha_i}{\beta_{i+1}} = \exp\left(-\frac{W_{i+1} - W_i}{kT}\right) \tag{27}$$

Equations 24, 26, and 27 are used to evaluate the rate constants for the ith transition pair. Reflecting boundary

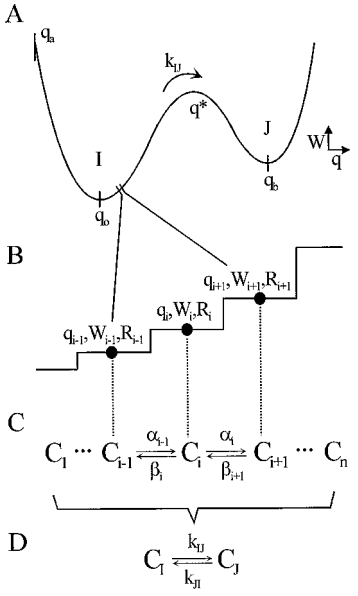

FIGURE 1 Schematic of spatial coarse graining procedure applied to a bistable diffusion model (*A*). The potential of mean force (pmf) landscape is discretized into increments of Δq resembling a staircase (exploded view in *B*). Computation of gating kinetics requires formulating the Smoluchowski equation (Eq. 1) into a master equation (*C*), for which the set of rate constants α_i, β_i are computed from the gating charge displacement (q), pmf (W), and resistance (R), using Eqs. 24 and 27. The next step in coarse graining generates a two-state DSM model (*D*), which accurately predicts gating kinetics on the slow time scale of transition events. The forward rate constant k_{IJ} is computed as the reciprocal of the mean first passage time from point q_o in state I of the diffusion landscape to an absorbing site q_b in state J. A reflecting barrier at q_a prevents leftgoing transitions for the case in which there exist additional states in that direction. The backward rate constant k_{JI} (not shown) is obtained in similar fashion. The region near q^* is the transition state of the energy barrier.

conditions at the charge positions $q = 0$ and $q = q_{max}$ arise automatically because the master equation describes a closed system. Absorbing boundaries are useful when computing conditional transition rates out of a metastable well (see next section). Left- and right-sided absorbing boundaries are obtained by letting α_1 and β_n approach zero, respectively.

The nondiagonal entries of the "Q"-matrix **A** describing the master equation are $a_{ij} = \alpha_i \delta_{j,i+1} + \beta_i \delta_{j,i-1}$. The transpose of **A** is comparable to the Fokker-Planck operator **F,** making **A** the adjoint of **F** in the limit $\Delta q \to 0$. Once the rate constants have been found and charge displacements assigned to each state, the problem of the gating particle diffusing along a piecewise continuous energy and friction landscape is reduced to solving the master equation, as outlined in the Theory section.

Macroscopic transition rates in barrier models

We have stated that a diffusion model with large barriers can be represented by a DSM model for the slow time scale of activated transition events. This statement must obviously be quantified with regard to the size of transition barriers and the valid range in time scales for which it holds true. To do this we refer to Fig. 1 and define the conditional transition rate $k_{IJ}(t)$ as the probability that, within the period between times t and $t + dt$, the gating particle reaches an absorbing boundary q_b in state J, given that it began at $t = 0$ from point q_o in state I. A defining feature of a Markovian state is that the value of conditional exit rate "constants" be independent of dwell time for the time scale of interest. A standard expression in reliability theory (Papoulis, 1991; Liebovitch et al., 1987) is that the conditional rate is obtained from the waiting time probability distribution $P_I(t)$ through the relation

$$k_{IJ}(t) = -\frac{d}{dt} \ln P_I(t) \tag{28}$$

$P_I(t)$ is found by first converting the region from q_a to q_b into an n-state master equation. The rate constant $\beta_{n,n-1}$ is then set to zero, making state n at point q_b perfectly absorbing. The approximate expression for $P_I(t)$ is then given by (Millhauser et al., 1988)

$$P_I(t) = \sum_{j=1}^{n-1} p_j(t) \tag{29}$$

where p_j are the state probabilities. Given initial conditions $p_i(0)| = \delta_{ij}$, where $i = q_o/\Delta q$, then, by diagonalizing the transition matrix **A** and combining the right-sided eigenvectors into the matrix $\mathbf{M} = \{|\mathbf{v}\rangle\}$, Eq. 29 may be written as

$$P_I(t) = \sum_{j=1}^{n-1} \sum_{r=1}^{n} m_{ir} m_{rj}^{-1} \exp(\lambda_r t) \tag{30}$$

where m_{ij} and m_{ij}^{-1} are elements of **M,** and $\mathbf{M}^{-1}$, respectively and the set of λ's are the eigenvalues. Applying Eq. 28 to Eq. 30, the conditional transition rate is given by

$$k_{IJ}(t) = \frac{-\sum_{j=1}^{n-1} \sum_{r=1}^{n} m_{ir} m_{rj}^{-1} \lambda_r \exp(\lambda_r t)}{\sum_{j=1}^{n-1} \sum_{r=1}^{n} m_{ir} m_{rj}^{-1} \exp(\lambda_r t)} \tag{31}$$

Examples of the time course of $k_{IJ}(t)$ using different barrier heights appear in the Results.

Equation 31 may also be used for another purpose, namely the calculation of opening rates versus dwell times (k_{CO} versus t_C) for single-channel ionic current data. Such measurements have served as a test for the presence or lack of barriers in the energy landscape (Liebovitch et al., 1987). To calculate single-channel opening rates, Eq. 31 is used with the modification that $i = n - 1$, where n is presumed to be the open state.

If one is reasonably sure that a transition is Markovian, a much easier method of calculating a unidirectional rate constant k_{IJ} is to calculate the mean first passage time T_{IJ}, defined as (Gardiner, 1990)

$$T_{IJ} = \int_0^\infty P_I(t) dt \tag{32}$$

The solution of Eq. 32 for the Smoluchowski equation is (see Gardiner, 1990, for a more general expression of mean first passage times)

$$T_{IJ} = \frac{1}{kT} \int_{q_o}^{q_b} R(q') \exp\left(\frac{W(q')}{kT}\right) dq' \int_{q_a}^{q'} \exp\left(\frac{-W(q'')}{kT}\right) dq'' \tag{33}$$

which is readily computed through numerical integration. For large transition barriers, the rate constant is the reciprocal of the mean first passage time. A practical feature of Eq. 33 is that it easily handles discontinuities in $R(q)$ and $W(q)$.

Given a piecewise harmonic energy profile, and assuming constant friction, the expression for the rate constant assumes a familiar form, namely Kramers' large friction approximation (Gardiner, 1990):

$$k_{IJ} \approx \frac{\sqrt{cc^*}}{2\pi R} \exp\left(-\frac{W(q^*) - W(q_o)}{kT}\right) \tag{34}$$

where $c = W''(q_o)$ and $c^* = -W''(q^*)$. The prefactor in Eq. 28 is an agreeable alternative to the commonly employed "universal rate constant" kT/h, the latter being inappropriate even for Eyring's absolute rate theory, from which it was borrowed, and which requires additional knowledge of partition functions (Eyring, 1935; Chen et al., 1997).

METHODS

Units

We elected to express quantities in units appropriate for the size of molecular events seen on the physiologic time scale. The most relevant are

time, in milliseconds (ms); charge, in electronic units (eu = 1.602×10^{-19} coulombs); and voltage, in millivolts (mV). Other units are expressed in terms of the preceding three. For example, energy has units of millielectron volts (meV = eu · mV). The temperature in all cases is assumed to be 290.11 Kelvin, for which the thermodynamic energy kT = 25 meV, where k is Boltzmann's constant. A useful conversion factor for current is 1 fA = 6.2415 eu/ms.

Numerical methods

Numerical and Monte Carlo analyses were performed either on a Pentium 60 PC or a 500-MHz DEC Alpha computer, using computer programs written in standard C language. Certain numerical algorithms, such as matrix routines, random number generation, eigenvalue decomposition, and splining operations, were taken directly with little or no modification from Press et al. (1992). Numerical computation of mean gating currents and their autocorrelations use Eq. 10a–c. Computing time was saved by summing only over significant eigenvalues, which were determined (for example) in the mean gating current by terminating the summation when the accumulated charge movement $\Sigma_r \rho_r$ changed less than one part in a million over five additions. Time-dependent quantities were "sampled" at discrete intervals, $1/f_s$, where f_s was typically five times greater than the cut-off frequency f_c of the subsequent filtering operation. Sampling and filtering in the time domain are discussed in detail below. Quantities for which frequency is the independent variable (such as the power spectrum) were computed without filtering, so as to make visible the entire frequency spectrum. Monte Carlo simulations were sampled and filtered in a fashion comparable to that of the numeric calculations. Thus, assuming numerical errors due to sampling, round-off, large step size, etc. were kept to a minimum, the two methods superimposed exactly in their prediction of gating currents and their fluctuations. The details of Monte Carlo simulation are shown below.

Sampling and filtering

The effects of sampling and filtering must be carefully considered when computing gating currents using the numerical methods described under Theory. Aliasing artifacts can lead to distortions of the predicted results. This is particularly true of the autocorrelation function, which is intimately related to the power spectrum in the frequency domain, where aliasing is classically characterized. However, increasing the sample rate is not necessarily the remedy of choice, as there will always exist eigencomponents in a diffusion model that decay more quickly than may be practically sampled. The situation is best appreciated by considering gating currents generated from a barrier landscape. As was mentioned earlier, large barriers produce gating events on widely separate time scales. Fast events occur on the diffusive time scale, whereas events occurring in the physiologic time domain are typically slower by two or more orders of magnitude. Modeling most experimental data requires sampling on a slow time scale, but many components of the gating current will have decayed before the first sampling interval is complete. The effect is minor when the mean gating current is computed, where only the fast initial transient is affected. However, large errors can occur in computing the autocorrelation function, which mixes fast eigenvalues into the expression of slow components, causing significant distortion of the signal, even at long times.

The key to preventing sampling artifacts is to introduce a correction factor for each eigencomponent that gives the correct Riemann sum area, and then digitally filter with an operation that maintains area. Digital filtering was performed by convoluting the discretized signal with a Gaussian kernel, as described by Colquhoun and Sigworth (1995). For a sampling rate of f_s, and a −3 db cutoff frequency f_c, the filtered gating current and autocorrelation were computed in digitized form as

$$\hat{\mu}[k] = \sum_{u=0}^{h_m} \mu[k-u] \cdot h[u] \tag{35a}$$

$$\hat{C}[k_1][k_2] = \sum_{u,v=0}^{h_m} C[k_1-u][k_2-v] \cdot h[u] \cdot h[v] \tag{35b}$$

where $h_m \approx f_s/f_c$, and $f_s \geq 5f_c$. The filtering kernel $h[k]$ is the time response to a Kronecker delta function. It is Gaussian with standard deviation $\sigma = (\ln 2)^{1/2} h_m/2\pi \approx 0.1325\, f_s/f_c$:

$$h[k] = \delta[k] = \frac{1}{\sqrt{2\pi} \cdot \sigma} \exp\left(-\frac{(k-T)^2}{2\sigma^2}\right) \tag{36}$$

The discrete time lag $T = h_m/2$ corresponds to $1/(2f_c)$ in real time. The Gaussian digital filter is a fairly good approximation to a high-order analog Bessel filter, which is commonly used in time domain electrophysiologic recording because of its linear phase response (Leib and Pasupathy, 1992). For $h_m \geq 5$, the kernel satisfies, to within 5% error,

$$\sum_{k=0}^{h_m} h[k] = 1 \tag{37a}$$

$$\sum_{k=0}^{h_m} h^2[k] = \sqrt{\frac{\pi}{\ln 2}} \frac{f_c}{f_s} \equiv \frac{2B}{f_s} \tag{37b}$$

where the "effective" bandwidth $B \approx 1.064\, f_c$ (Crouzy and Sigworth, 1993). The unfiltered mean current and autocorrelation function were calculated according to

$$\mu[k] = \sum_r \omega_r \zeta_r \exp(-k\phi_r) \tag{38a}$$

$$C[k_1][k_2 \geq k_1] = \sum_r \chi_r \zeta_r \exp(-k_1\phi_r) f_s \delta_{k_1,k_2} \tag{38b}$$

$$+ \sum_{r,s} \upsilon_{rs} \zeta_r \exp(-k_1\phi_r) \zeta'_s \exp(-(k_2-k_1)\phi_s) \tag{38c}$$

$$C[k_2][k_1] = C[k_1][k_2] \tag{38d}$$

where $\phi_r = -\lambda_r/f_s$ is a positive quantity. Following Crouzy and Sigworth (1993), we refer to Eqs. 38b and 38c, respectively, as the "delta" and "correlation" terms of the autocorrelation function. The sampling rate f_s in the delta term is needed to produce the factor $2B$ in the filtered result, as is evident from Eq. 37b. The correction factors ζ_r and ζ'_r are defined as the ratio of the exact integrals, $\int_0^\infty \exp(-\phi_r t)dt$ and $\int_{-\infty}^{\infty} \exp(-\phi_r|t|)dt$, respectively, divided by their left-sided Riemann sums, where the time increment is equal to the reciprocal of the sampling rate. The explicit expressions are

$$\zeta_r = \frac{1-\exp(-\phi_r)}{\phi_r}$$
$$\zeta'_r = \frac{2(1-\exp(-\phi_r))}{\phi_r(1+\exp(-\phi_r))} \tag{39}$$

As was mentioned, the purpose of the scaling factors is to normalize the area of the discretized signal so that the subsequent filtering operation will produce the correct time course of the signal. In the case of a barrier model, the fast diffusion components appear as delta functions on the physiologic time scale. The filtering operation converts these spikes into an impulse response spread out in time, but there must be the proper "weight" attached to each to prevent size distortion. The correction factors given by Eq. 39 provide the correct scaling for the discretized signal.

Monte Carlo simulation

Sample trajectories of a diffusive variable may be obtained through discretization of a stochastic differential equation equivalent to the Smoluchowski equation. The standard approach uses a discrete time version of a Langevin equation with a spatially dependent noise term, where stochastic integration is performed with a Runge-Kutta scheme. Following Rumelin (1982), a second-order algorithm, which, depending on the value of a weighing term ϵ, converges to one of several desired stochastic interpretations, is given by

$$q_{i+1} = q_i + \tfrac{1}{2}[g_1(q_i) + g_1(\hat{q}_{i+1})]\Delta t + [(1-\epsilon)g_2(q_i) + \epsilon g_2(\hat{q}_{i+1})]\Delta Z_i \quad (40)$$

where the Euler increment is

$$\hat{q}_{i+1} = q_i + g_1(q_i)\Delta t + g_2(q_i)\Delta Z_i \quad (41)$$

ΔZ is an increment of the Wiener process for the time difference Δt, whose probability density function is given by

$$g(\Delta Z) = \frac{1}{\sqrt{2\pi\Delta t}} \exp\left(-\frac{\Delta Z^2}{2\Delta t}\right) \quad (42)$$

Operationally, each ΔZ_i is generated by drawing a number from the standard normal distribution and multiplying by $\Delta t^{1/2}$. To simulate the Langevin equation, we use the following expressions for g_1 and g_2:

$$g_1(q) = \frac{-W'(q)}{R(q)} \quad (43a)$$

$$g_2(q) = \sqrt{\frac{2kT}{R(q)}} \quad (43b)$$

For this choice, setting ϵ to unity causes the simulation to converge to the result given by the Smoluchowski equation. In performing the simulations, the time interval Δt was chosen so that any given change in the pmf over one time interval did not exceed a certain percentage of the activation barrier height, i.e., $W(q_{i+1}) - W(q_i) < \alpha E_a$, where α was usually 1%. During the simulation, the number of violations of this rule was tallied, and Δt was decreased if the frequency of violation was greater than one in 10^6. Reflecting boundary conditions were obtained by checking at every increment whether the value of q had exceeded the boundaries and, if so, by placing it back at the corresponding endpoint. Absorbing boundaries are obtained by simply halting the simulation at the time of exit of the specified region.

To initiate a simulation, the initial value q_1 of the trajectory was randomly drawn from the Boltzmann distribution $C \exp(-W(q, V_o)/kT)$. Because the time increment Δt is in the diffusive regime ($\sim 10^{-7}$ s), a single run lasting 10 ms will contain ~100,000 data points. To keep the file sizes manageable, a decimation procedure was performed. For a sampling frequency f_s, one in every $(f_s\Delta t)^{-1}$ points was kept. Digital filtering before sampling prevented aliasing artifacts. An enormous reduction in filtering time is achieved by filtering only with respect to the sampled points q_j. Gating currents were then calculated by discrete differentiation: $i_j = f_s(q_j - q_{j-1})$. Individual trajectories were added to a running sum to produce an ensemble average. In some cases, an ensemble variance was also calculated. The accuracy of the simulation was often checked by comparing the mean current $\langle i(t) \rangle$ from dual trials, using different values of Δt. Comparisons with the numerical computation provided a further check.

RESULTS

We now illustrate the theory with a series of examples.

The harmonic well

The first model is the simple yet historically important case of the one-dimensional harmonic oscillator (Ühlenbeck and Ornstein, 1930). The harmonic oscillator has a parabolic pmf profile, which is the simplest representation of a symmetric potential well. By studying the properties of a gating particle subject to a linear restoring force, one may, to a first approximation, predict the characteristics of the fast gating event. The explicit form of the pmf is given by

$$W(q) = aq^2 - qV \quad (44)$$

where the constant a has units of inverse capacitance, and V is the applied voltage. We will in general refrain from discussing mechanistic models, but a simple representation of the oscillator is a charged particle attached to a spring, surrounded by a viscous linear dielectric medium. Control over the bulk electric field can be achieved with large capacitor plates charged through an external feedback circuit that supplies the necessary current to keep the voltage difference constant.

Gating currents predicted by the oscillator model were obtained numerically for the following values: $R = 0.5$ mV · ms/eu, $a = 250$ mV/eu. These values were chosen to match the gating current to the time course of the fast early component seen in the *Shaker* potassium channel (Stefani and Bezanilla, 1996). The voltage protocol consisted of a step at time $t = 0$ from a holding potential $V_h = -50$ mV to the test pulse $V_t = 0$ mV. Reflecting barriers were placed at positions $q = \pm 1$ eu, limiting the trajectory space of the gating particle. Although we computed 300 eigencomponents from a 300-state discretization scheme, only the first harmonic (with eigenvalue: λ_f) significantly contributed to the mean gating current. This was expected because the theoretical gating current for an overdamped harmonic oscillator has a single exponential time course. The decay rate ($-\lambda_f$) was computed to be 1000.2 kHz, very near the theoretical value of $2a/R = 10^3$ kHz. This is much faster than can be resolved with conventional voltage clamp setups and explains why the fast gating event, which has a comparable relaxation rate, usually goes unnoticed in gating current experiments.

Monte Carlo simulations based on the discretized Langevin equation can be used to visualize the random Brownian motion of an individual gating particle within a harmonic well (Fig. 2, *top*). The trajectories are highly irregular, and the single channel gating current (Fig. 2, "i") bears no resemblance to an exponential decay. Nonetheless, the ensemble average of 50,000 sweeps clearly reveals the underlying exponential tendency of the gating particle's motion (Fig. 2, "μ"). The ensemble variance, on the other hand, is entirely stationary (Fig. 2, "var"). This is consistent with the spectral properties of the harmonic oscillator, whose single-sided power spectrum is voltage independent and has the form

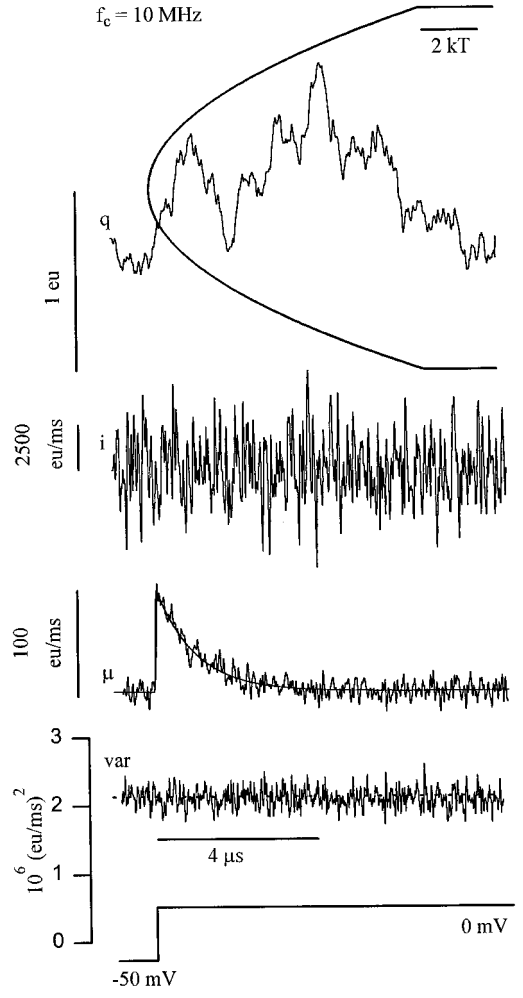

FIGURE 2 The overdamped harmonic well. Monte Carlo and numerical predictions of gating currents filtered at 10 MHz in a simulated voltage clamp experiment ($V_h = -50$ mV, $V_t = 0$ mV). A typical trajectory of the gating charge displacement (q) produces a gating current (i) with random diffusion noise. Superimposed on the trajectory of q is the pmf profile at 0 mV. It is given by the parabolic function aq^2, where $a = 250$ mV/eu. The ensemble mean of 50,000 current traces is shown superimposed on the numerical mean (μ, *smooth line*). The ensemble variance (var) fluctuates around the Nyquist value of $4ktB/R = 2.13 \times 10^6$ (eu/ms)^2 at the dotted line.

of a high-pass filter:

$$S(\omega) = \frac{\omega^2}{\omega^2 + \lambda_f^2} \frac{4kT}{R} \tag{45}$$

The high frequency limit of Eq. 45 is the Nyquist value of $4kT/R$. It can be shown that for the overdamped system with constant resistance, the Nyquist value is a good approximation of the high frequency limit of the single-sided spectrum for any choice in energy landscape, regardless of the shape of its profile. Because of the large recording bandwidth used in the simulation ($\omega_{max} \gg \lambda_f$), the value of the variance may be approximated by $4kTB/R$, where B is the effective bandwidth of the filter (see Methods for the definition of bandwidth). As shown in Fig. 2 (*bottom*), this approximation is in close agreement with the simulation result. It should be noted that the voltage independence of the gating current variance does not extend to very large voltages, because under these conditions the gating particle favors the boundary regions, which decreases fluctuations. In electrophysiologic parlance this is known as "saturation," for which the experimental manifestation is a flattening of the mean charge displacement versus voltage (Q-V) curve outside the capacitive region. This is an important feature of real channels, because it implies that the gating apparatus is a closed system, as it should be if gating charge is a permanent part of the channel protein.

Single-barrier model

Starting with the harmonic well as our benchmark for a diffusion process, it may be altered in one of two ways such that it generates macroscopically observable gating events for a much slower (physiologic) time scale. Either frictional resistance must be increased, or barriers are introduced into the energy landscape. A greater resistance lowers the mean drift velocity of the random walk but adds nothing new to the dynamics, except to slow down the process and decrease the Nyquist (diffusion) noise. On the other hand, energy barriers introduce new dynamics that are chiefly apparent on a slower time scale.

The single-barrier model was constructed by placing two harmonic wells side by side, separated by a 150-meV ($6kT$) barrier in the shape of an inverted parabola (Fig. 3, *top*). This is the classic bistable system considered by Kramers (1940) in his seminal paper on reaction rate theory. Here, the fast diffusive motion inside the wells is virtually identical to the previous oscillator model, but now the possibility of transitions over the barrier produces additional large-scale (macroscopic) fluctuations at lower frequencies, the kind predicted by a DSM model with two states.

The values of the forward (k_1) and backward (k_2) transition rate constants of the representative two-state DSM model were estimated from Kramer's approximation (Eq. 34), as well as from the reciprocal of barrier mean first passage times (T_{mfp}, Eq. 33). Because the pmf profile is piecewise harmonic, the two methods gave similar predictions. With the slow time behavior being determined from a single rate constant pair, the current response to a voltage step on the physiologic time domain is monoexponential. However, with the full range of time scales taken into account, the single barrier model combines features from both the harmonic well and the discrete two-state model. This is best appreciated by comparing weighing terms evaluated for gating currents predicted by each of the respective models—the harmonic well, the two-state DSM model, and the single-barrier continuum model (Tables 1–3). Only the most significant eigencomponents (shown in bold) of the two continuum models (Tables 1 and 3) are included. The weighing terms for the DSM model can be written in closed form as a function of the rate constants (α_1, β_1) and the

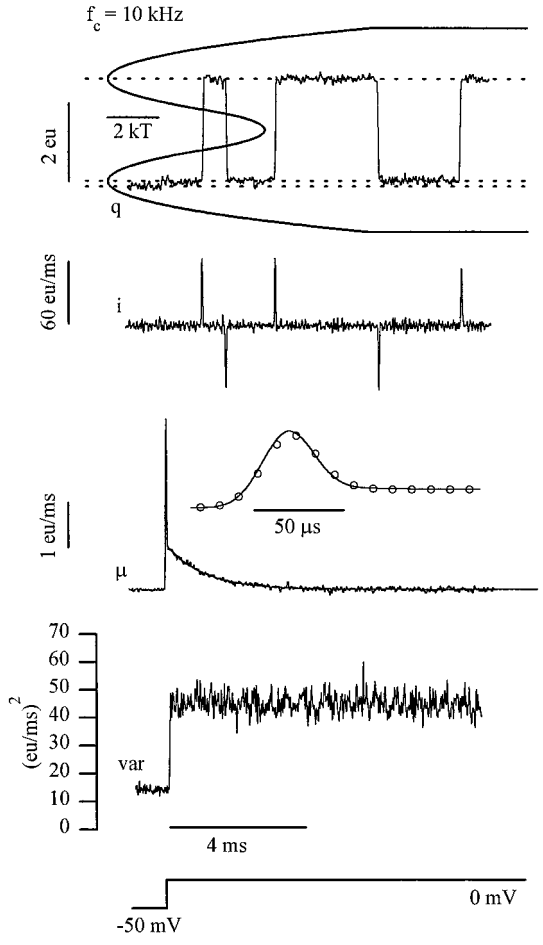

FIGURE 3 The single-barrier model constructed from two harmonic wells connected by an inverted parabolic barrier. The protocol for Monte Carlo and numerical predictions was identical to that in Fig. 2, except for a 1000-fold decrease in bandwidth (f_c = 10 kHz). Dotted lines superimposed on the energy profile indicate local regions of energy minima before (*lowest line*) (*upper two lines*) and after the step to 0 mV. The slow time scale of observation causes barrier transitions in (*q*) to appear instantaneous, generating bandwidth limited spikes in the gating current (*i*). The underlying diffusion noise that is visible between transition events has been greatly diminished, as compared to Fig. 2, by the reduced bandwidth. Numerical calculations of the mean gating current (μ, *smooth line*) agrees well with the ensemble mean of 50,000 current traces (*noisy line*). The predicted early fast event (*inset,* ensemble points given by *unfilled circles*) is the filtered output of the fast oscillator relaxation shown in Fig. 2. The value of the ensemble variance (var) is dominated by diffusion (Johnson or Nyquist) noise at −50 mV and shot noise at 0 mV.

transition charge, $\Delta q = 2$ eu. They are, for a step to 0 mV (see Eq. 13 for notation), $\omega_s = k_1\Delta q$, $\chi_o = 2k_1k_2\Delta q^2/(k_1 + k_2)$, and $\upsilon_{os} = -k_1k_2\Delta q^2$, where it is assumed for simplicity's sake that the first state holds 100% of the starting probability density (the actual value was 98%, but the 2% discrepancy has little effect on the results). The remaining DSM weights are identically zero. Directing our attention to the first three eigencomponents of the single-barrier model, the corresponding eigenvalues at 0 mV are λ_o (equilibrium) = 0, λ_s (slow) = $k_1 + k_2$, and λ_f (fast) = $2a/R$. It is apparent from Tables 1–3 that the single-barrier model has weighing

TABLE 1 Eigencomponents for the harmonic oscillator model (V_h = −50 mV, V_t = 0 mV)

υ_{uv}	v = o	v = *f*	ω_u	χ_u
u = o	0	**−50,160**	-8×10^{-10}	**100.3**
u = f	-8×10^{-8}	0	**100.0**	-1×10^{-7}

$\lambda_o = 0$, $\lambda_f = -1000.2$.

TABLE 2 Eigencomponents for the discrete two-state model (V_h = −∞, V_t = 0 mV)

υ_{uv}	v = o	v = s	ω_u	χ_u
u = o	0	**−0.972**	0	**1.972**
u = *s*	0	0	**0.986**	0

$\lambda_o = 0$, $\lambda_s = -0.986$, $1/T_{mfp} = 0.493$ kHz.

factors in common with the other two models. The zeroth delta weight, χ_o, is an interesting case in that its computed value is similar to that of the harmonic well, but we can obtain the value predicted by the DSM model from the expression $\chi_o - 2\upsilon_{of}/\lambda_f$. As discussed in the Methods, this is possible because "correlation" terms that mix fast and slow eigencomponents are effectively equivalent, in the physiologic time domain, to "delta" terms (Eq. 38b), which decay at a rate given by the slow eigenvalue. As a result, the single-barrier continuum model predicts delta correlated current (white noise) for two ranges in frequency, slow and fast, which are evident as plateaus in corresponding regions of the power spectrum (Fig. 4).

The nature of gating current fluctuations predicted by a barrier model is best seen in Monte Carlo simulations performed at physiologic bandwidths (10 kHz). In a sample trajectory obtained from the single-barrier model shown in Fig. 3 (*top*), transitions are marked by gating current spikes whose area is equal to the amount of gating charge displaced (Fig. 3, "i"). The duration of a typical transition event is so brief that, on the physiologic time scale, the transition spikes appear as the impulse response of the filter, which preserves area. These spike-induced fluctuations produce shot noise (Rice, 1944) and are responsible for the low frequency shoulder seen in the power spectrum (Fig. 4). The underlying Brownian motion fluctuations remain visible between the transition spikes, but, as is apparent from the power spectrum (Fig. 4, *dashed line*), this background noise is greatly attenuated at physiologic bandwidths as compared to the diffusion time scale (compare Figs. 2 and 3, trace "q"). The ensemble mean of 50,000 trajectories (Fig. 3, trace "μ") clearly displays evidence of the expected two gating current components: the slow exponential component predicted by the discrete two-state model, preceded by the impulse response of the fast exponential decay.

Estimate of elementary charge movement

We investigated the response of the single-barrier model to positive voltage steps, expecting it to behave like a DSM

TABLE 3 Eigencomponents for the single-barrier model (V_h = −50 mV, V_t = 0 mV)

v_{uv}	v = o	v = s	v = f	ω_u	χ_u
u = o	0	**−0.976**	**−49,161**	-2×10^{-11}	**100.3 (2.07)***
u = s	-2×10^{-11}	0	8.491	**0.953**	1×10^{-4}
u = f	-2×10^{-9}	−0.017	0	**98.7**	2×10^{-5}

$\lambda_o = 0$, $\lambda_s = -0.988$, $\lambda_f = -1000.9$.
*Value in parentheses: $\chi_o - 2v_{0f}/\lambda_f$.

model for moderate voltages that preserve the barrier height, but not for extreme depolarizations. At the moderate potential of +50 mV, the original 150-meV height of the transition barrier is decreased by a third in the forward direction and increased by a third in the backward direction. These modest changes in barrier height preserve the separation of eigenvalues into "slow" and "fast" categories—thus the model retains its two-state character (Fig. 5 *A*). Transition rates in kHz estimated from mean first passage times at −50 mV were $k_1 = 3.02$ and $k_2 = 0.056$, in reasonable agreement with the numerical estimate of the first nonzero eigenvalue $\lambda_1 = -3.11$, which, for a two-state model, is equal to $k_1 + k_2$. Because k_1 is 54 times larger than k_2, the gating process is largely irreversible in the forward direction. The relationship between mean current and variance of N independent irreversible two-state subunits is, in the high bandwidth case of $B \gg \lambda_1$ (Conti and Stühmer, 1989; Crouzy and Sigworth, 1993),

$$\mathrm{Var}(t) \cong 2B\Delta q_e \mu(t) - \frac{\mu^2(t)}{N} + C_b \qquad (46)$$

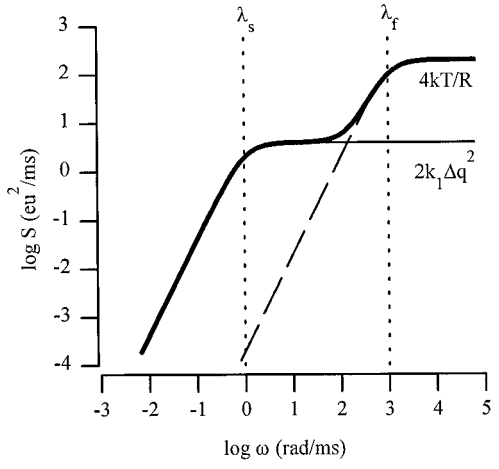

FIGURE 4 Equilibrium spectral analysis of the harmonic well, the single-barrier model, and the two-state DSM model. The power spectra of the three models are characterized by corner frequencies at two time scales, slow (λ_s) and fast (λ_f). The single-sided power spectrum of both the harmonic well (*dashed line*) and DSM model (*thin line*) are of the high-pass type. The high frequency limit of the harmonic well is the Nyquist value $4kT/R$. The two-state DSM model attains a power of only $2k_1\Delta q^2$, which exceeds that of the harmonic well at low frequencies, where shot noise is the dominant source of fluctuations. The single-barrier model (*bold line*) has characteristics of the harmonic oscillator at high frequencies and of the two-state DSM model at lower frequencies.

Equation 46 gives us a formula for estimating the elementary transition charge movement Δq_e, which in this case is ~2 eu. The constant C_b consists of diffusion noise in an ideal recording system. Amplification noise must also be added as a component of C_b when a physical recording system is utilized. We fitted the ensemble variance of 500 Monte Carlo traces to the mean current ($N = 100$) using Eq. 46 and estimated a value of 1.94 for Δq_e, confirming the irreversible two-state nature of the kinetics (Fig. 5 *C*).

Single-barrier with extreme depolarization

The two-state behavior of the single-barrier model is lost when we step to a large voltage. We should expect that, in physical systems, linear voltage dependence will eventually break down at extreme potentials. However, neglecting this possibility for a step to 500 mV, the energy landscape is tilted to such a degree that the barrier effectively disappears (Fig. 5 *D*) and drift motion predominates. This phenomenon has recently been observed in mechanical measurements of protein-ligand interactions by atomic force microscopy, where the potential barrier leading to bond rupture decreases with increasing cantilever position (Shapiro and Qian, 1997). During its brief traversal of the energy landscape, the gating particle moves with a drift velocity proportional to the slope of the energy profile. This explains the depression of the gating current ~1 μs into the pulse, at which time the probability distribution experiences a momentary slowdown as it moves across the scaled-down remnant of the original barrier (Fig. 5 *E*). Although the kinetics of the current has sped up considerably, the decay is not as rapid as predicted by the Arrhenius prediction of the rate constants:

$$k_1 = \upsilon \exp\left(\frac{\Delta qV}{2}\right)$$
$$k_2 = \upsilon \exp\left(-\frac{\Delta qV}{2}\right) \qquad (47)$$

where the value of υ is chosen so that decay rate, $k_1 + k_2$, matches that of the single-barrier model at $V = 0$. The Arrhenius values were compared to the diffusion-limited decay rates obtained from two standard methods, the reciprocal of mean first passage times and the value of the first nonzero eigenvalue. For very depolarized potentials, the diffusion-based values of the rate exhibited marked deviation from the Arrhenius prediction (Fig. 5 *F*). The mean first passage time proved to be a more accurate indicator of the time required to move $(e - 1)/e$ of the total charge movement than the eigenvalue method, because, as the barrier became less prominent, the single dominant eigenvalue of the two-state model gave way to a larger number of high-frequency eigenvalues, the smallest of which still overestimated the general "rate" of the process. Because the Arrhenius relationship is a cardinal feature of rate constants in DSM models, transition charges in DSM models must be

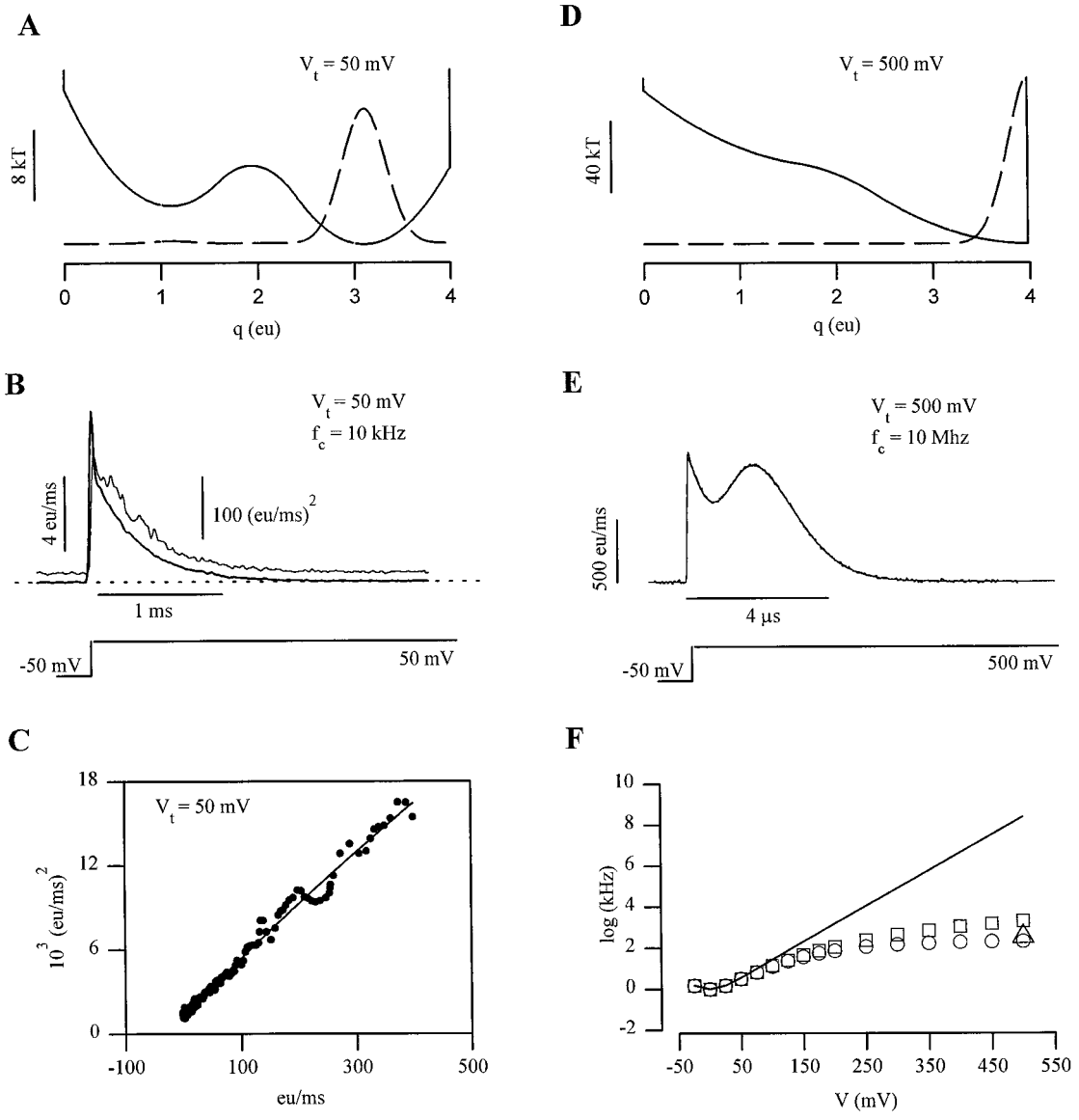

FIGURE 5 Gating currents predicted by the single-barrier model for steps to moderate (V = 50 mV) and extreme (V = 500 mV) potentials. The energy landscape retains the barrier in the moderate (*A*) but not the extreme (*D*) depolarization. (*B*) Ensemble mean (*bold line*) and variance (*thin line*) estimated by Monte Carlo simulation of 500 traces × 100 channels. (*C*) Mean-variance plot with fit by parabolic function to estimate the elementary charge movement (see text for details). (*E*) Monte Carlo (*noisy line*) and numerical calculations (*smooth line*) of the gating current in response to a 500-mV pulse. The shape of the gating current reflects drift motion of the gating particle. (*F*) Semilog plot of estimated time constant of relaxation (*circles:* mean first passage times; *squares:* first nonzero eigenvalues; *triangle:* reciprocal of time at which $(e - 1)/e$ of charge movement was complete) deviates from reaction rate theory (*smooth line*) at large depolarizations due to the grossly diminished activation barrier.

kept small to prevent the development of inappropriately large values of transition rates at the extremes of the voltage range (Schoppa and Sigworth, 1998). Diffusion models are less affected by this problem because they experience linear dependence of voltage at extreme potentials.

Time dependence of escape rate as a function of barrier height

In the preceding example, the single-barrier model strayed from its two-state character at some potential between 50 and 500 mV. The reason for the transition from discrete Markovian to diffusional drift behavior was loss of barrier height. But how does one quantitatively decide whether a state is Markovian? We investigated this problem for the case of V-shaped barriers of varying height by calculating conditional transition rates, as defined in the Theory section. The explicit meaning of a Markovian state is that the conditional rate leaving the state must be time independent. Plots of "escape" rates out of the state centered at q_o are shown in Fig. 6, where both abscissa and ordinate are normalized with respect to the mean first passage time. For this particular landscape, the state began to lose its Markovian character for barriers lower than $7kT$, evidenced by

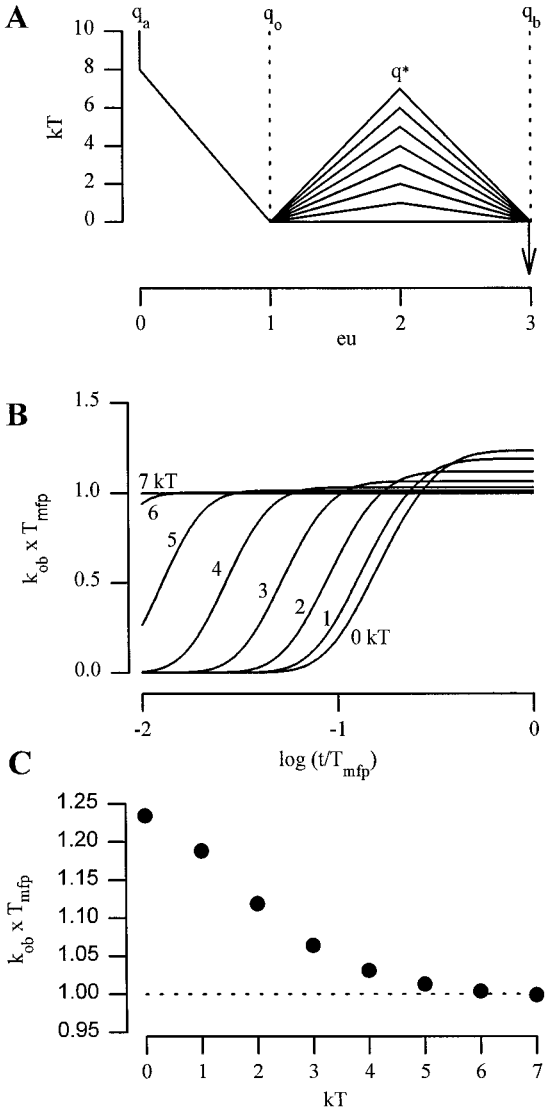

FIGURE 6 Quantifying the Markovian property of a metastable state. (*A*) Sawtooth-shaped landscapes with barrier heights ranging from zero to 8*kT*. Conditional "escape" rates from q_o to q_b with reflection at q_a were calculated as a function of dwell time (*B*) using Eq. 74. Both abscissa and ordinate were normalized with respect to the mean first passage time, T_{mfp}. The Markovian property of a time-independent escape rate is satisfied over two orders of magnitude in dwell time for barrier heights of 7*kT* or greater. The results were found to be independent of the value of the resistance. ***(C)*** The limiting values of rate constants are best approximated by $1/T_{mfp}$ for barrier heights greater than 5*kT*.

the time delay in reaching the steady-state value of the conditional rate, and the failure of the steady-state value to match the reciprocal of the mean first passage time. However, even the 4*kT* barrier predicted a rate to within 5% accuracy for dwell times longer than 10% of its own value. These results were found to be independent of the value of the friction coefficient, although they will of course vary somewhat with the shape of the well and the barrier. In conclusion, one should remember the simple rule: a "well-defined" Markovian state is primarily judged by the depth of its well, and barrier heights of at least 4–5*kT* are needed for a DSM representation to be approximately valid on a slow time scale.

Two-barrier model

By introducing additional barriers to the energy landscape of the single-barrier model, we can generate gating currents that resemble experimental recordings from voltage-dependent potassium and sodium channels. Each sufficiently large barrier (in the sense of the preceding section) adds a dominant slow exponent to the gating current. Some components of the mean gating current have a negative value, leading to an initial rise in the shape of the signal. This "rising phase" is a distinguishing feature of gating currents in several biological channels. In the traditional state kinetic model, at least three states are needed to model such a current. Simply put, the requirement for a rising phase in the gating current predicted by a sequential two-barrier model is that the initial transition moves less charge and/or has a smaller forward rate constant than the following transition (Bezanilla and Taylor, 1982).

An example of a model that produces a rising phase is the double barrier scheme shown in Fig. 7 *A*. Starting from state I, transition I $\rightarrow$ II has a larger barrier and smaller charge step than transition II $\rightarrow$ III. Assuming that the channel is in state I at the beginning of the pulse, this asymmetric landscape leads on average to a long waiting time until the first transition to state II. This event is marked by a spike in the gating current (Fig. 7 *B*, trace "i"). The first transition event is followed relatively quickly by a second event, which generates a larger current spike than the first. Backward transitions are less frequent (although not rare) because of the greater activation energy in the reverse direction at $V =$ 30 mV. Because many trials in a series of Monte Carlo simulations occur just as described, the slow time course of the mean gating current begins with a rising phase (Fig. 7 *C*, *upper trace*). Preceding the slow events is the ubiquitous fast component of the gating current produced by the rapid equilibration of probability density within state I. The inset of Fig. 7 *C* shows what the fast component looks like with a 10-MHz recording bandwidth. It has an approximately exponential time course despite the fact that state I, from which the fast component arises, is approximated poorly by a parabola. The entire kinetics of the process can be summarized by the semilog plot of component charge displacement versus eigenvalue (Fig. 7 *D*, *circles*). The separation of eigenvalues into "slow" and "fast" groups is quite evident, with the slow time behavior containing only two eigencomponents. The slow pair of eigencomponents are nearly identical to those predicted from the three-state DSM representation, obtained from the rate constants k_{12}, k_{21}, k_{23}, and k_{32}, which in turn were calculated by taking mean first-passage times across barriers in the continuum model (Fig. 7 *D*, *triangles*). The grouping of fast eigencomponents contribute in total only 2.4% of the total charge movement in the continuum model, the remainder appearing in the slow components of gating.

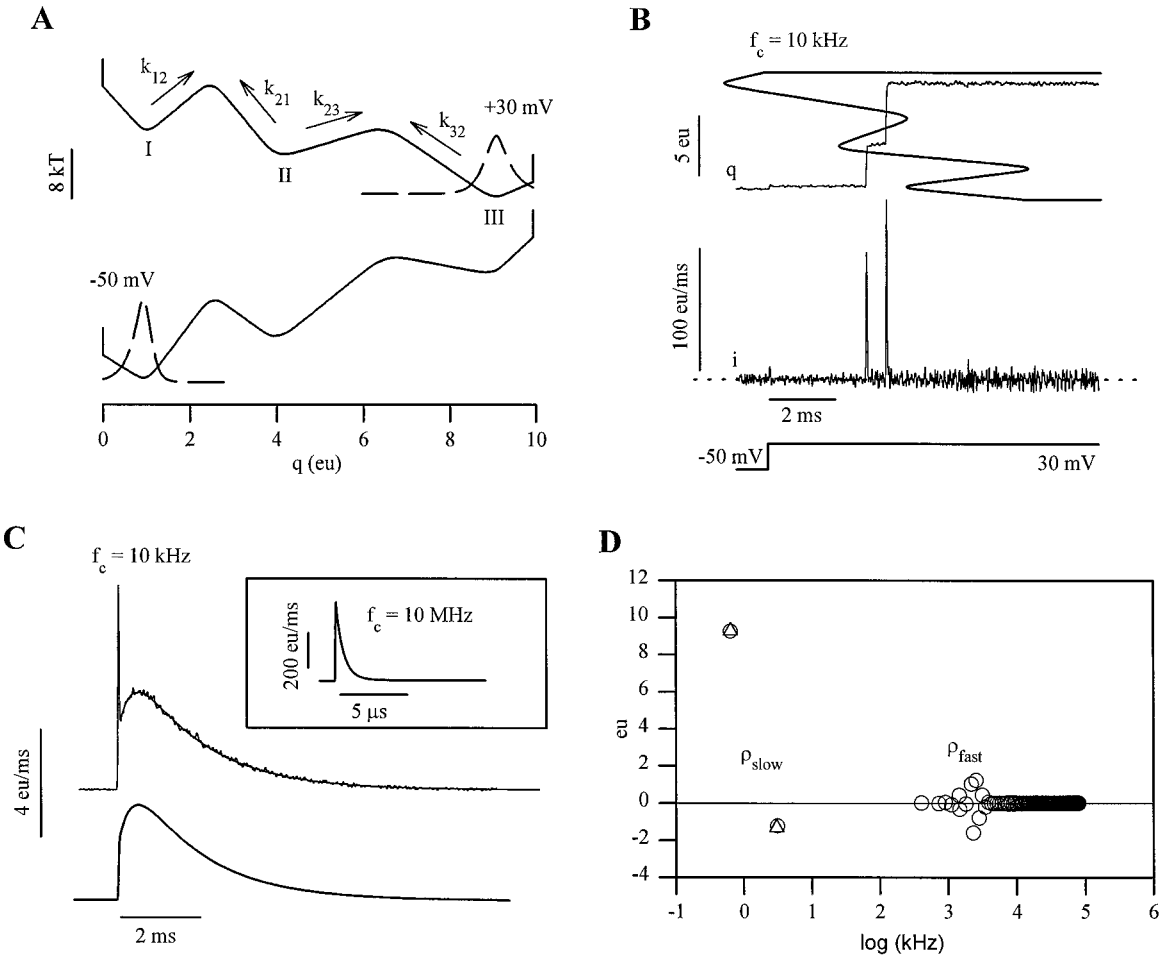

FIGURE 7 Double-barrier model. (*A*) Potential profiles shown for −50 mV and +30 mV with equilibrium distributions of the most populated states (*dashed lines*). The three metastable states are labeled I, II, and III. The unidirectional rate constants labeled by the arrows were calculated from first mean passage times and used to construct a three-state DSM model. (*B*) Single trajectory of charge displacement (q) and current (i) for a pulse to 30 mV. The origins of the early fast event and the subsequent rising phase of the slow current are evident from the size and timing of the current spikes in this "typical" trace. Note that whereas the early event nearly coincides with the voltage step, the occurrence of transition spikes is randomly distributed. (*C*) Comparison of gating currents from the double-barrier model (*top,* superimposed Monte Carlo and numerical calculations) with the corresponding DSM model (*lower trace*) demonstrates nearly identical slow time behavior. The early fast component of the gating current predicted by the continuum double-barrier model is shown at 10-MHz bandwidth in the inset. It is still visible at 10 kHz, although it could easily be mistaken for unsubtracted membrane capacity transient. The DSM model does not produce a fast gating component. (*D*) Semilog plot of component gating charge movements ($\rho_i = -\omega_i/\lambda_i$) versus nonzero eigenvalues (*circles:* continuum model; *triangles:* DSM model).

"Barrier" versus "drift" models

We wanted to see if a barrierless landscape could predict the slow gating current kinetics of the two-barrier model for a single value of the applied potential. To find such a model, we increased the value of the resistance to 100-fold that of the two-barrier model (to $R = 20$ mV · ms/eu) and then attempted to fit the gating current predicted by the two-barrier model by varying the location of nine points along a continuous energy landscape. The fitted points were connected via a smoothing function to produce a continuum of states (Fig. 8 *B*, trace "d"), and from this continuum model, gating currents were calculated and compared to the original. The fitting procedure was performed by modifying ScoP model generation software (Simulation Resources, Barrien Springs, MI) to incorporate the external source code for the eigenvalue and filtering routines described in the Methods section. The charge positions of the first eight points were spaced 1 eu apart, leaving the value of the final charge displacement a free variable. The entire set of energy values were left free except the first, which was set arbitrarily to zero. We found that, to reproduce the shape of the rising phase, the resting potential had to be more hyperpolarized (−90 mV). Otherwise, at a resting potential of −50 mV, the initial probability distribution was spread across too much of the energy landscape, activating a large number of eigencomponents, resulting in a blunted rising phase. The value of the last charge position was adjusted to produce the correct area under the curve, i.e., the total charge movement. The fit duplicated admirably the slow components of the gating current, but the fast transient could obviously not be

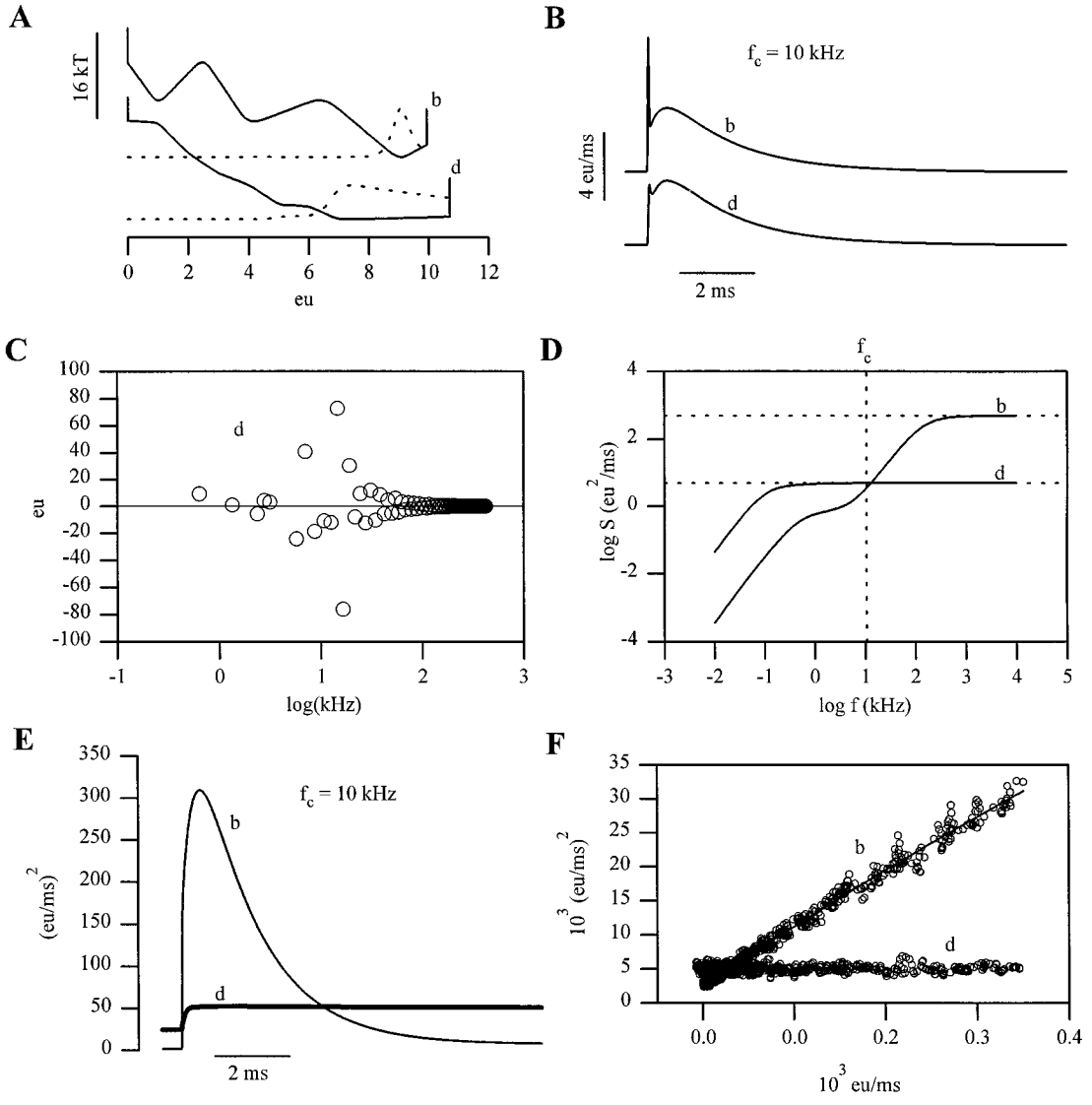

FIGURE 8 Characteristics of a drift model (*d*) predicting a slow gating current similar to that of the double-barrier model (*b*) at 30 mV. (*A*) Landscapes are shown for both models at 30 mV with equilibrium probability distributions (*dashed line*). (*B*) Predicted gating currents (barrier model: −50 to 30 mV, R = 0.2 mV-ms/eu; drift model: −90 to 30 mV, R = 20 mV-ms/eu). The difference in the gating current lies primarily in the fast component, which is significantly slower in the drift model because of the larger resistance. (*C*) Plot of charge components versus eigenvalue derived for the gating current in *B* of the drift model. There is no clear separation in time of eigencomponents as there was in Fig. 7 *D*. (*D*) Predicted power spectrum at 30 mV, with horizontal dotted lines marking the Nyquist limit ($4kT/R$) of both models. The single vertical dotted line marks the 10-kHz cut-off frequency of the recording filter. The spectrum of the barrier model has a shoulder in the physiologic time domain reflecting transition induced shot noise. (*E*) Variance traces corresponding to the mean currents in *B*. The nonstationary component of the barrier model (*thin line*) rises significantly above the small increase predicted by the drift model. (*F*) Mean-variance plots of Monte Carlo simulations with 100 channels. The slope of the fit to the barrier model (*smooth line*) is consistent with an elementary charge movement predicted from Eq. 16 (details in text). In contrast, the variance of the drift model is independent of the value of the mean current.

reproduced with such a large value of the resistance (Fig. 8 *A*, "d").

As anticipated, the barriers present in the original model (Fig. 8 *B*, "b") nearly disappeared as a result of the increased resistance (Fig. 8 *B*, "d"), suggesting that the motion of the gating particle no longer occurs in discrete jumps on the physiologic time scale, but instead would be best described as diffusive drift. This is confirmed by the distribution of exponential weights (Fig. 8 *C*), which is spread more evenly over a wide range of frequencies. Comparing the power spectra of the two models, the barrier model has a shoulder from 1 to 10 kHz due to transition-induced shot noise (Fig. 8 *D*, "b"), whereas the drift model has already reached the Nyquist regime at 1 kHz (Fig. 8 *D*, "d"). Despite the fact that the equilibrium value of the variance is slightly higher at 10 kHz, the nonstationary noise predicted by the drift model is relatively constant, consistent with diffusive motion (Fig. 8 *E*, "d"). In contrast, the nonstationary variance of the barrier model rises to more than 500 times the equilibrium level, reflecting the large fluctuations produced

by "shot" events that were initiated by the step change in voltage (Fig. 8 *E*, "b").

The plot of the decay phase of the variance generated by the barrier model versus the mean gating current was fit to a parabolic function similar to Eq. 46. The fit was quite linear, and the value of the elementary charge movement was estimated to be $q_e = 4.14$ eu (Fig. 8 *F*, "b"). By comparison, the first and second transition charge movements in the double-barrier model were 3.2 eu and 4.8 eu, respectively. Inserting these latter values into the approximate formula for elementary charge movement given by Eq. 16, we obtain a value of 4.16 eu. This close agreement with the fit result should not be taken too seriously, however, because of the numerous approximations made in deriving Eq. 16. The concept of elementary charge movement is, of course, meaningless for the drift model, and in any case, the lack of time evolution in the variance prevents the mean-variance plot from yielding useful information. In fact, it prevents the variance from being measured at all, because only the nonstationary component of the variance can be distinguished from background noise in actual experiments.

Position-dependent resistance

The conclusion reached so far is that, for large friction models of ion channel gating, uncorrelated gating current noise arises in two circumstances. If the energy landscape has large barriers, we observe primarily shot noise for bandwidths that are comparable in value to the slow group of eigenvalues. Under these conditions, the time course of the variance can be computed from the rate constants and transition charge displacements that describe the projected DSM model. On the other hand, landscapes without macroscopic barriers produce predominantly Nyquist noise. If we assume, as we have thus far, that R is independent of position, then the ability to measure nonstationary noise is solely consistent with a barrier model. However, Nyquist noise can be made to change with time if we make the R position dependent.

Consider the following heuristic attempt at constructing a drift-like model with nonstationary noise. We would like the magnitude of the variance to reflect a Δq_e of two electronic charges, reflecting the estimates of 1.7–2.4 eu that have been measured in sodium and potassium channels (Conti and Stühmer, 1989; Sigworth, 1993; Sigg et al., 1994). A gating particle quickly reaches its terminal drift velocity ($W'(q)/R$) when placed on a uniform energy gradient. The gating current variance has the Nyquist value of $4kT/R$. Using Eq. 15 as a working definition of the elementary charge movement, we calculate its value for a gating particle experiencing pure drift to be

$$\Delta q_e = \frac{\mathrm{Var}(t)}{2B\mu(t)} \approx \frac{2kT}{W'(q)} \tag{48}$$

It appears that applying a 25-mV (= kT/eu) voltage to a flat energy landscape would produce the desired value of Δq_e, a result that is independent of the value of the resistance. However, the resistance needs to change in time for the Nyquist noise to be distinguishable from background noise. With these ideas in mind, we experimented with the model shown in Fig. 9 *A*. The spatially inhomogeneous resistance has a large value at the ends of a 12-eu-long landscape, decaying exponentially from both sides to a broadly based minimum at about the middle of the landscape. The pmf at 0 mV is flat for small values of the gating charge displacement, but dives down at a rate of 50 mV/eu, beginning at $q = 8$ eu. The energy "trap" thus created forces the equilibrium probability distribution to populate the high-resistance area at the far end of the landscape, which results in a small Nyquist noise at the end of the pulse. Starting with a holding potential of −80 mV, application of a pulse to 25 mV causes the gating particle to begin to drift toward positive values of the gating charge displacement. It eventually reaches the region of low resistance, where it moves more quickly, producing large fluctuations, as seen in the representative trajectory ("q") of Fig. 9 *B*. Eventually, as the gating particle passes into the trap, the rise in resistance dampens the fluctuations. The plot of mean gating current versus variance estimated from numerical and Monte Carlo analysis has approximately the desired slope of 2 eu in the decay phase (Fig. 9 *C*). Surprisingly, the slope remains relatively constant over a wide range of depolarized potentials (less than 25% change from 20 mV to 100 mV), which does not follow from Eq. 48, which predicts an inverse relationship between Δq_e and the applied voltage. However, a similar insensitivity of the elementary charge movement to voltage is seen experimentally in *Shaker* potassium channels for depolarized potentials (unpublished data). There was, in addition, a qualitative similarity to real gating currents in potassium channels (Bezanilla et al., 1994) when ON and OFF traces were calculated for test pulses ranging from −100 mV to 50 mV. There are, of course, differences in kinetic detail between experiment and the model, most noticeably in the shape of the OFF trace, but so far the only serious attempts at fitting gating currents have employed DSM models, for which large barriers are implicitly assumed. It remains to be seen if, with a little effort, simple "drift" models with position-dependent friction can be made to accurately reproduce gating current data.

The full autocorrelation function

Following the suggestion by Crouzy and Sigworth (1993) that the shape of the nonstationary autocovariance function might be used to distinguish between kinetic schemes, we computed the complete single-channel autocovariance function for the double-barrier model and the inhomogeneous friction model, applying different voltage protocols to make the general time course of the kinetics about the same for both models. Evaluating the autocovariance near the occurrence of a step change in potential (t_o) is tricky because eigencomponents from both resting and test potentials are

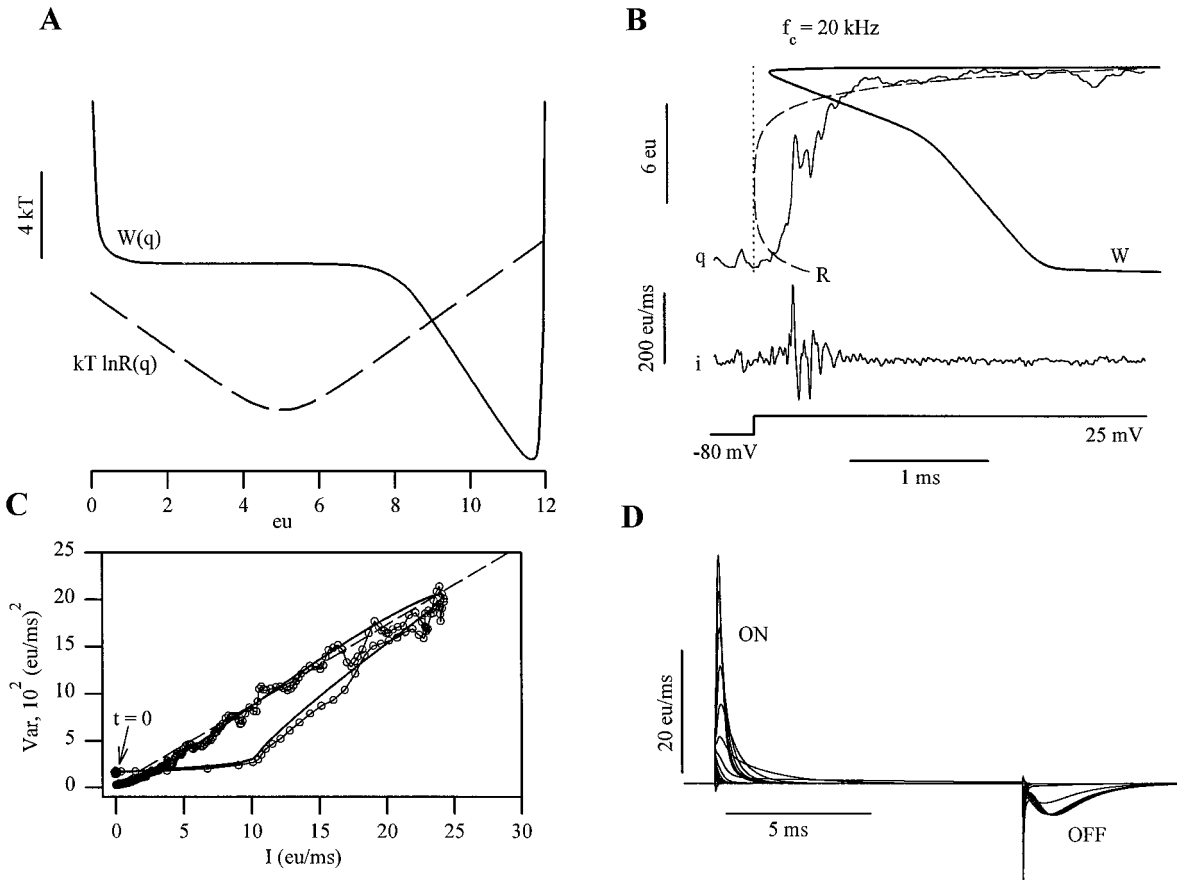

FIGURE 9 Drift model with inhomogeneous resistance. (*A*) Contributions to the effective energy are the pmf $W(q)$, which determines the equilibrium probability distribution, and the "spurious drift" potential, kT ln $R(q)$ (*dashed line*). (*B*) Monte Carlo trajectory of the gating charge displacement (q) superimposed on the pmf (W) and the resistance profile (R, *dashed line*). Traversal by the gating particle across the low-resistance region results in large fluctuations in gating current (i). (*C*) Plot of mean current (I) versus variance (Var) for the entire duration of the voltage protocol in *B*. Smooth line: Numerical calculation. Circles: Ensemble mean and variance of Monte Carlo simulation (10-μs intervals). Dashed line: $2B\Delta q_e I$ + Var(∞), for Δq_e = 2 eu, B = 21.28 kHz, and Var(∞) obtained from numerical calculation. (*D*) Predicted activation gating currents (ON) and deactivation currents (OFF) for test pulses ranging from −100 mV to 50 mV from a holding potential of −80 mV.

involved. To resolve the difficulty we used the Markovian property $\mathbf{P}(t_1 < t_o, t_2 > t_o) = \mathbf{P}(t_1, t_o)\mathbf{P}(t_o, t_2)$ to find transition probabilities spanning t_o and rederived Eqs. 10 and 11, using these mixed transition probabilities. The characteristic features of the autocorrelation term in both models consisted of a bandwidth limited spike at the reference point and positive correlations at both earlier and later times (Fig. 10). The reference spike is largely a manifestation of "shot" noise in the case of the barrier model, whereas in the drift model it is due purely to uncorrelated Nyquist noise. The positive correlations outside the reference time can be explained by the relative lack of backward transitions in the barrier model, or by the directed motion in the forward direction caused by the tilting of the drift landscape. In contrast to the autocorrelation function, the complete autocovariance does not demonstrate positive correlations outside the reference spike. This is due to a subtracting term consisting of the product of the mean currents. The autocorrelation function is not a cumulant of the gating current and thus does not scale linearly with the number of channels N. However, if N is known from total gating charge per channel experiments (Schoppa et al., 1992; Aggarwal and MacKinnon, 1996; Seoh et al., 1996), then the single-channel autocorrelation function may be derived from the autocovariance and the mean gating current, which *are* cumulant functions. The relationship is

$$N\,\mathrm{corr}(t_1, t_2) = \mathrm{Cov}(t_1, t_2) + \frac{I(t_1)I(t_2)}{N} \qquad (49)$$

where I and Cov are the mean and autocovariance of N independent channels, and corr is the single-channel autocorrelation function. Although the autocorrelation is worth studying in more detail, there are no obvious qualitative differences between the autocorrelations in Fig. 10; both the barrier model and the drift model with inhomogeneous resistance have the delta spike and positive correlations, making it difficult to discriminate between barrier versus inhomogeneous drift models.

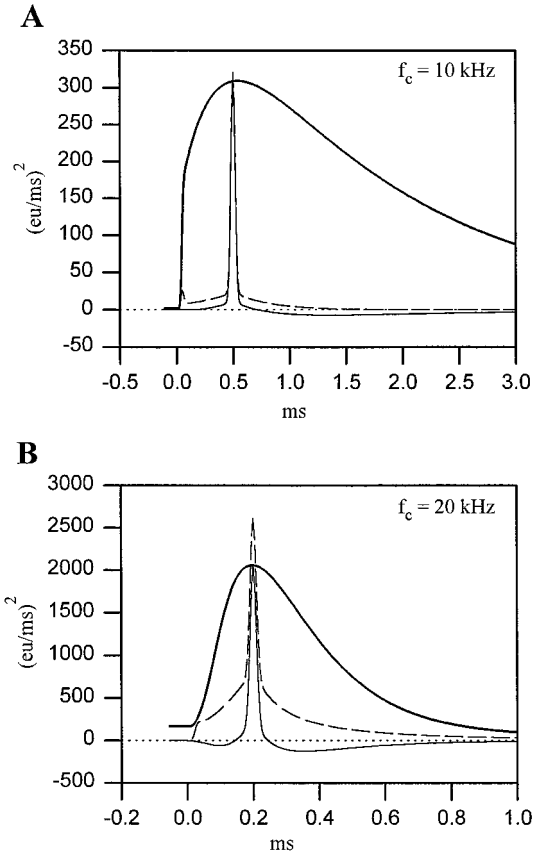

FIGURE 10 Autocovariance (*thin line*) and autocorrelation (*dashed line*) functions computed for a single reference time, superimposed on the time course of the variance (*bold line*). (*A*) Double-barrier model ($V_h = -50$ mV, $V_t = 30$ mV, $f_c = 10$ kHz). (*B*) Drift model with inhomogeneous resistance from Fig. 9 ($V_h = -80$ mV, $V_t = 25$ mV, $f_c = 20$ kHz). The bandwidth limited spike at the reference time and positive correlations in the gating current are characteristics common to both models.

Spectral analysis of an eight-state model

In the absence of explicit knowledge about the pmf of a channel, the distinction between drift and barrier gating processes may be best appreciated by examining their spectral properties. Defined loosely, spectral analysis involves finding marked changes in a signal at specific frequencies that correspond to the eigenvalues of the dynamic process. For example, the dominant transition of the single-barrier model manifested itself in the appearance of a low-frequency shoulder in the power spectrum of the simple harmonic well (Fig. 4). In general, there are $n - 1$ dominant eigenvalue frequencies for n stable states in a barrier model, although they may be difficult to tease apart experimentally if they are spaced too closely together. Drift models tend to have a high density of eigencomponents in the physiologic time domain, consistent with a diffusion process.

We will now examine the spectral properties of a barrier diffusion model derived from a published DSM scheme describing the equilibrium and kinetic properties of gating charge displacement from the *Shaker* potassium channel in the range of potentials −66 to −18 mV (Bezanilla et al., 1994). The rationale for doing so is to see whether a multiple-barrier diffusion model with gating properties similar to those of a real channel has a spectral signature that can be easily distinguished from that of a drift model, which always produces a smear of eigenvalues. The published DSM model had seven sequential nonconducting states followed by an eighth conducting (open) state. Rate constants and gating charge displacements were specified for every forward and backward transition. We constructed a diffusion model with similar kinetic properties by connecting energy coordinates of the DSM model in sawtooth fashion along the charge displacement axis. Relative transition state energies were obtained from the rate constants through an Arrhenius equation with an arbitrary prefactor. This sawtooth landscape underwent smoothing operations (Methods) and was rescaled, so that, together with a judicious choice of the constant value resistance ($R = 0.5$ mV · ms/eu), the resultant diffusion model (Fig. 11 *A*) generated reasonable looking gating currents on the physiologic time scale (Fig. 11 *B*) and on the diffusive time scale, where it reproduced the early event (Fig. 11 *B*, *inset*).

We employed three methods of representing the diffusive eight-state model in the frequency domain. They are shown in Fig. 12 for the same range in frequencies. Fig. 12 *A* plots the component charge displacements as a function of eigenvalue for a pulse from −90 mV to 10 mV. Although there are eight discernible transition barriers in the energy diagram, only six of seven possible components dominate the slow frequencies at 10 mV. The less than expected amount of eigencomponents is explained by the fact that positive depolarization renders state C6 unstable and prone to immediate forward transitions because of marked lowering of the energy barrier from C6 to C7. In other words, C6 at 10 mV is no longer a stable Markovian state. To a lesser extent, the same is true for the low barrier between the open state and C7, creating a fast, partly diffusive equilibrium between the two states.

Theoretically, all eigencomponents should be apparent in time domain records of gating currents, so that obtaining the rate constants and charge displacements of the equivalent DSM model becomes a matter of solving the inverse problem. However, in practice it is exceedingly difficult to reliably extract more than three exponential decays from a single time course unless the time constants are spaced widely apart. Thus more information is needed from other measurement modalities.

The most common method of spectral analysis is the computation of the power spectrum (Fig. 12 *B*). This may be obtained experimentally through fluctuation analysis of gating currents under conditions of thermal equilibrium, although in practice it should be easier to infer it from admittance measurements, which are less sensitive to contaminating background noise. In any case, the numerically derived power spectrum from the diffusive eight-state model at 10 mV poorly separates out the individual eigencomponent because of the large number of corner frequencies in a relatively narrow frequency band. The slow com-

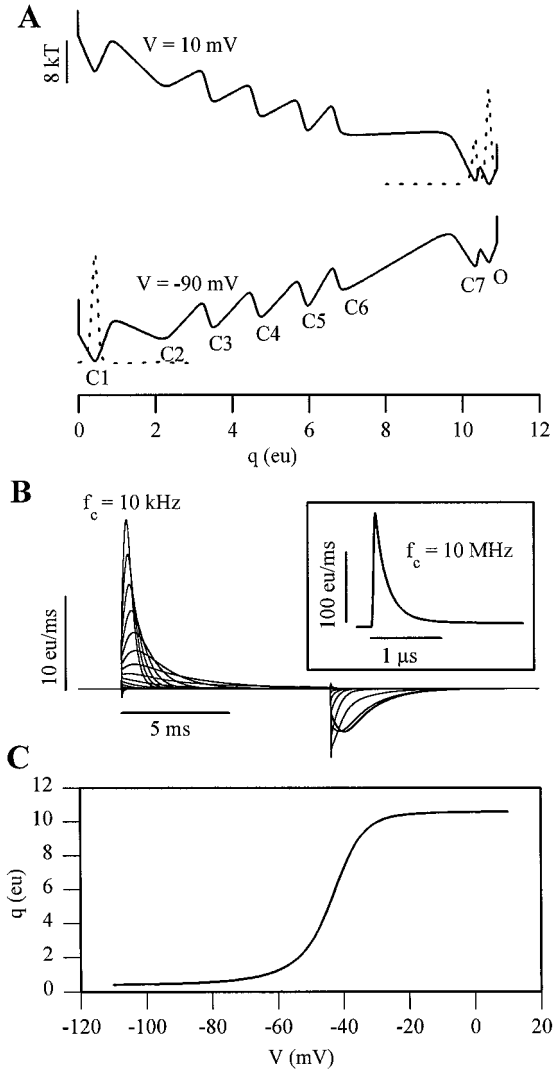

FIGURE 11 Continuum model with eight metastable states. (*A*) The pmf profile shown at hyperpolarized (−90 mV) and depolarized (+10 mV) voltages. The dashed line is the probability distribution for the most populated states. The open (conducting) state is labeled O. (*B*) Numerical computation of gating current series at 10-kHz bandwidth with test pulses to the range of voltages: −120 mV to +30 mV, with 10-mV intervals, and a holding potential of −90 mV. The inset shows the early component of gating from a step to 10 mV at high bandwidth (f_c = 10 MHz). (*C*) The equilibrium charge displacement versus voltage (*Q-V*) curve of the eight-state model.

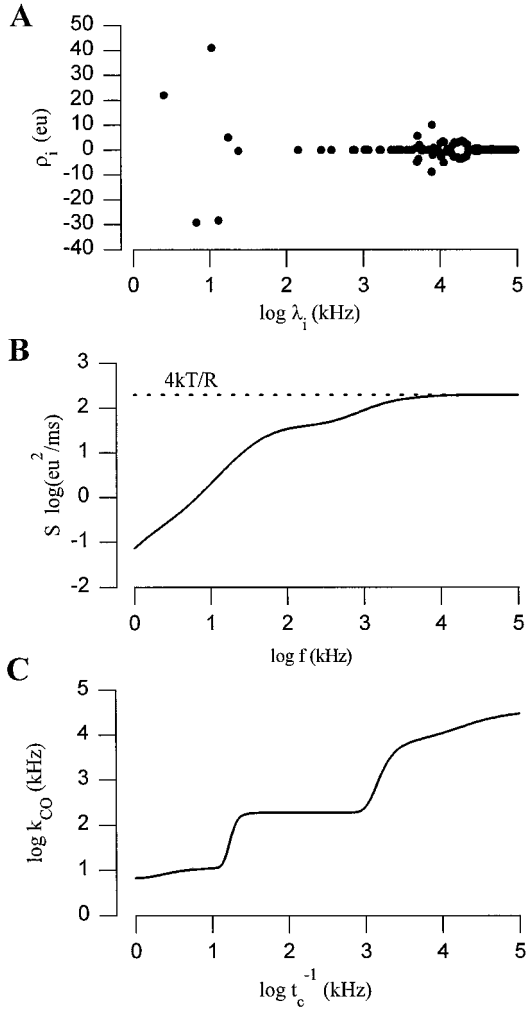

FIGURE 12 Spectral analysis of the eight-state model in Fig. 11. (*A*) Semilog scatter plot of 176 gating current eigencomponents for a voltage step from −90 mV to +10 mV. Abscissa: eigenvalue; ordinate: component gating charge movement ($\rho_i = \omega_i/\lambda_i$). The fast component is made up of the cluster of points in the vicinity of 10^4 kHz. (*B*) Power spectrum at +10 mV. The high-frequency limit is indicated by the dotted line labeled $4kT/R$. (*C*) Log-log plot of opening rate (k_{CO}) versus reciprocal closed time duration ($t_{C^{-1}}$), where opening is defined as being to the right of the midline of state O in Fig. 11 *A*. Long closed times are caused by sojourns deep in the closed state space, producing plateaus in the value of the effective rate constant for small values of $t_{C^{-1}}$. The sustained rise of the plot at the upper range of frequencies is due to fast diffusion near the open state.

ponents of gating combine to form a broad shoulder appearing below the Nyquist limit.

A potentially more informative technique is the log-log plot of the rate of opening versus dwell time of opening (k_{CO} versus t_C), which requires single-channel ionic recordings (Liebovitch et al., 1987; McManus et al., 1988). Using Eq. 31, and placing an abrupt transition to open at the bottom of state O, we plotted the logarithms of k_{CO} versus $t_{C^{-1}}$ at 10 mV. In this plot (Fig. 12 *C*), there are noticeable plateaus at discrete values of the time-dependent rate of opening, the clearest suggestion so far of a barrier model, although at large frequencies ($t_{C^{-1}} > 3.5$ kHz) the curve rises steadily, analogous to what was demonstrated by Millhauser et al. (1988) for a drift landscape. The smooth rise of the plot at high frequencies is due to extremely brief (and extremely difficult to measure) closed times, in which the gating particle never leaves the initial well, demonstrating the existence of diffusive behavior in a barrier model. Of course, any single-channel analysis is heavily weighed toward transitions near the open state, because closed states far removed from the open state are less likely to be sampled. However, despite this limitation, measuring conditional opening rates as a function of dwell times is a useful technique for detecting barriers in a localized region of the energy landscape.

DISCUSSION

We have presented a model of voltage-dependent gating in ion channels based on the Smoluchowski diffusion equation. Although in certain cases the predicted gating behavior is well represented by the traditional discrete-state Markov (DSM) model, there are fundamental advantages in considering a more detailed configuration. The strengths of diffusion based theory are 1) it predicts drift motion, whether it be the early gating event, friction damping at extreme potentials, or the motion of the gating particle across a drift landscape, all of which can be experimentally tested; 2) energy plays an integral role in the dynamics, which greatly simplifies equilibrium thermodynamics and facilitates the crucial link between detailed physical mechanisms of gating and the kinetics of ion channel activation; 3) it paints a more realistic picture of large-scale protein dynamics than the Eyring-based transition state theory currently in use. Some weakness of the approach are 1) the additional computational workload needed to predict kinetics, although we have managed to speed up the numerical routines to the point that we can fit experimental data to diffusion models; 2) it remains a phenomenological theory without basis in channel structure; 3) the voltage dependence of the potential energy profile may deviate significantly from linearity because of shielding interactions with ions in the bulk solution. Once the details of the geometry and mechanism of channel gating become clearer, and assuming that solution ions fluctuate more rapidly than components of the gating apparatus, the voltage dependence of the charge distribution and energy profile can be estimated from solving the nonlinear Poisson-Boltzmann equation. Amendments to the theory, such as adding an extra dimension to the energy landscape or a time-dependent friction kernel, can be implemented as required.

Diffusion theory versus DSM and fractal models

There has been spirited debate in recent years over the validity of DSM models in describing closed time distributions of certain channels over a large time scale (Korn and Horn, 1989; Liebovitch, 1989; McManus et al., 1989). In these channels, the logarithm of the opening rate (k_{co}) descended smoothly over four orders of magnitude of the logarithm of the dwell time (t_c), a pattern referred to as "fractal" scaling. Physical mechanisms have been put forth to explain this behavior (Millhauser et al., 1988; Läuger, 1988; Condat and Jäckle, 1989). In the language of this paper, the fractal pattern of closed time distributions is predicted by a drift landscape lacking barriers. On the other hand, studies using large data sets of single-channel records taken from a different group of channels demonstrated distinct plateaus in the log-log plots (McManus et al., 1988), consistent with a barrier landscape possessing distinct Markovian states. Hence, the slow time scale gating kinetics of this second group of channels should be well described by a DSM model. However, as shown in Fig. 12 *C*, even a barrier model demonstrates fractal-like behavior over a definite range of frequencies. As barriers become less prominent, the log-log plot becomes smoother. It is possible that barriers in some channels are lower than in others, leading to self-similar scaling of single-channel records. In any case, by employing a diffusion approach, the discussion over which type of model is valid, fractal or DSM, can be replaced by asking what shape of the energy landscape is required to fit the data.

Repeated mention has been made of the inability of DSM models to describe the early gating event seen in *Shaker* and the sodium channel (Stefani and Bezanilla, 1996; Forster and Greeff, 1992). The early event is a persistent feature of high bandwidth recordings, and its kinetics are relatively insensitive to starting potential and temperature, features expected from rapid drift motion inside metastable states. The details of the early gating event await further characterization, but for now they appear entirely consistent in shape, voltage dependence, and time course with the fast equilibration occurring in a barrier model after a step pulse in voltage.

A prediction of the diffusion model that begs experimental investigation is the behavior of the gating current decay rate at extreme potentials ($>$200 mV). DSM models with Arrhenius-like rate constants predict that the decay rate rises exponentially with voltage. The exponential behavior continues until the magnitude of the half-barrier voltage drop approaches that of the height of the lowest barrier, at which point no more predictions can be made. Conversely, in a barrier diffusion model, the motion of the gating particle is drift limited as the barrier height vanishes (see Fig. 5, *E* and *F*). The value of the potential at which one observes a transition in a diffusion model from exponential to linear voltage dependence will be useful as an estimate of the barrier height corresponding to the rate-limiting step in gating. For instance, if the transition occurs at 400 mV, and if the rate-limiting barrier has a half-width of one electronic unit, then the height of the barrier is $\sim$400 meV, or $\sim 16kT$. Furthermore, from a modeling standpoint, drift limiting behavior at extreme potentials obviates the need to assign small charge displacements to transitions as a means of minimizing excessively rapid increases in transition rates (Schoppa and Sigworth, 1998).

Free energy versus rate constants

The transition state theory of Eyring gained instant popularity after the first efforts to use it to describe gating kinetics (Eyring et al., 1949). The result is that rate constants are used as the principal variables in phenomenological models of gating. The reason for this is understandable, because it is generally transient phenomena that are being recorded. If thermodynamic data on gating charge displacement were more widely available, then perhaps more models would be based on configurational free energy. In constructing a model, an effort should be made to describe it in terms of its configurational energy if at all possible, even if it is primarily the kinetic data that are of interest. There are several practical reasons for this. First, one must always be aware of the steady-state behavior of a gating system, which generally obeys detailed balance (i.e., is in equilibrium)

unless it is somehow connected to an external source of energy (Starace et al., 1997). For a rate constant description, this means checking that the product of rate constants in the clockwise and counterclockwise directions of any loop are equal, often requiring that one assign a calculated value for a single rate constant so that equilibrium conditions are satisfied. On the other hand, by specifying configurational energies, detailed balance is automatically ensured for any closed system. Furthermore, the partition function for an energy-based system is readily calculated, yielding simple expressions for the equilibrium probability distribution and relevant thermodynamic quantities (Conti, 1986). In contrast, the expressions for the same quantities expressed as rate constants are often unwieldy, and it may be difficult to express meaningful relationships between one quantity and another in complete generality (for example, the relationship between gating charge displacement and activation charge; Sigg and Bezanilla, 1997).

Many-body system with interactions

An additional advantage of an energy-based description is in dealing with complex interactions within a many-body system. An example relevant to the discussion of gating currents in real channels is the motion of the putative voltage-sensing domain, the S4 transmembrane segment, of which there are four in all known voltage-dependent channels. A common representation of the kinetic behavior of such a system is the classic Hodgkin and Huxley (HH) model of the potassium channel (Hodgkin and Huxley, 1952), made up of four noninteracting two-state gating particles (in this case, the S4 segments). The kinetic behavior of each subunit is generally described in terms of its forward and backward rate constants. The total configuration space for this system contains $2^4 = 16$ states, but because of degeneracies in the configuration space, it can be reduced to a five-state linear model with the well-known incremental sequence of rate constants. A further step in complexity is the Aldrich and Zagotta model (Zagotta et al., 1994), which assumes three states for each independent subunit, leading to $3^4 = 81$ individual states, which can again be reduced to a 15-state triangular model, although with a bit more difficulty as compared to the HH model. Schoppa and Sigworth (1998) have recently published a four-subunit model with four states per subunit. This leads to an increasingly unwieldy 256 states, which, in the absence of symmetry-destroying subunit interactions, condense to 35 individual states. The state diagram is now sufficiently complicated that it must be represented in three dimensions for purposes of illustration, and yet even this model may underestimate the number of states a single subunit may sample.

A more realistic description of gating is to assume that the S4 segments travel across space in a continuous manner, but the pathway may be described approximately by a sequence of an arbitrary number of positions, let's say 100. The configurational space now has a dimension of 10^8. Add to that the interactions of each of the seven charged amino acids in each S4 segment with one another and with the ions in the solution (the minimum representation imaginable), and a model based on transition rates becomes infeasible.

Now consider the same model from the viewpoint of an energy description. In contrast to the difficulty of obtaining a complete set of rate constants, the potential energy of each of the 10^8 configuration states can be computed in a relatively short time, even with intersubunit and subunit-solution electrostatic interactions taken into account. Each state is characterized by two values: the configurational energy ϵ and the charge displacement. To reduce the state description to a manageable size, a suitable binning process is applied to the configuration space to produce a smaller set of macroscopic states (100–300 states). The free energy W_i and charge displacement q_i of the ith macrostates are obtained from the subpartition function: $g_i = \Sigma_r \exp(-\epsilon_r/kT)$, where the index r is restricted to the ith group of configuration states. W_i and q_i are given by

$$W_i = -kT \ln g_i$$
$$q_i = kT \frac{\partial \ln g_i}{\partial V} \tag{49}$$

It can be readily demonstrated that the new state variables given by Eq. 49 predict exactly the same equilibrium conditions as the complete microscopic description, as can be easily verified in the case of the HH model. Computation of rate constants between macrostates requires more thought, however, because we have carefully avoided the use of transition rates until now. However, if the density of states is suitably large (the exact number depends on the steepness of the energy gradient, but can be as few as 40 states for a drift landscape), the ansatz given by Eqs. 24 and 26 may be used, where the set of resistance values R_i is chosen in such a way that the system decays within a reasonable time, and more importantly, that the kinetics of the overall process reduces to that of independent subunits when subunit interactions are removed. Armed with a complete description of the system in terms of a master equation, the numerical techniques described here can be used to compute ion channel behavior over a large range in time scales. Alternatively, if the system has well-defined metastable states, a Metropolis Monte Carlo procedure applied to the complete microscopic model can be used to evaluate "slow" transition rate constants across barriers by using the method of reactive flux (Chandler, 1978).

In conclusion, some form of diffusion theory is necessary to predict gating currents from a physical model characterized by strong solvent interactions. It is likely that the characteristic conformational motions of large, solvated proteins such as ion channels are significantly influenced by such interactions. Therefore, a reasonable approach to modeling ion channel kinetics requires diffusion theory. The next logical step is to find a physical model that successfully duplicates gating kinetics recorded from biological channels. In general, this necessitates replacing the phenomenological approach used here with a self-consistent theory (i.e., solving the Poisson-Boltzmann equation to obtain the

free ion distribution and the total system energy for small increments of gating charge configuration and voltage), although initially simplifying assumptions should be made to decrease the computational load. Eventually, the basic mechanism of the biological voltage sensor will be elucidated, although this awaits further advances in our knowledge of channel structure.

We thank Drs. Robert Eisenberg and Zeev Schuss for helpful discussions during the formative stages of this work, and members of the Bezanilla laboratory for comments on the manuscript. Supported by National Institutes of Health grant GM30376 and the Hagiwara Chair Fund. DS was also supported by Medical Scientist Training Program fellowship GM08042.

REFERENCES

Aggarwal, S. K., and R. MacKinnon. 1996. Contribution of the S4 segment to gating charge in the *Shaker* K^+ channel. *Neuron.* 16:1169–1177.

Bezanilla, F., E. Perozo, and E. Stefani. 1994. Gating of *Shaker* K^+ channels. II. The components of gating currents and a model of channel activation. *Biophys. J.* 66:1011–1021.

Bezanilla, F., and R. Taylor. 1982. Voltage dependent gating of sodium channels. *In* Abnormal Nerves and Muscles as Impulse Generators. W. Culp and J. Ochoa, editors. Oxford University Press, New York. 62–79.

Chandler, D. 1978. Statistical mechanics of isomerization dynamics in liquids and the transition state approximation. *J. Chem. Phys.* 68: 2959–2970.

Chen, D., L. Xu, A. Tripathy, G. Meissner, and R. S. Eisenberg. 1997. Permeation through the calcium release channel of cardiac muscle. *Biophys. J.* 73:1337–1354.

Colquhoun, D., and A. G. Hawkes. 1995. A Q-matrix cookbook: how to write only one program to calculate the single-channel and macroscopic predictions for any kinetic mechanism. *In* Single-Channel Recording. B. Sakmann and E. Neher, editors. Plenum Press, New York. 589–633.

Colquhoun, D., and F. J. Sigworth. 1995. Fitting and statistical analysis of single-channel records. *In* Single Channel Recording. B. Sakmann and E. Neher, editors. Plenum Press, New York. 483–587.

Condat, C. A., and J. Jäckle. 1989. Closed-time distribution of ionic channels: analytical solution to a one-dimensional defect-diffusion model. *Biophys. J.* 55:915–925.

Conti, F. 1986. The relationship between electrophysiological data and thermodynamics of ion channel conformations. *In* Ion Channels in Neural Membranes. Alan R. Liss. 25–41.

Conti, F., and W. Stühmer. 1989. Quantal charge redistributions accompanying the structural transitions of sodium channels. *Eur. Biophys.* 17:53–59.

Crouzy, S. C., and F. J. Sigworth. 1993. Fluctuations in ion channel gating currents: analysis of nonstationary noise. *Biophys. J.* 64:68–76.

Eyring, H. R. 1935. The activated complex in chemical reactions. *J. Chem. Phys.* 3:107–115.

Eyring, H., R. Lumry, and J. W. Woodbury. 1949. Some applications of modern rate theory to physiological systems. *Rec. Chem. Prog.* 10: 100–114.

Forster, I. C., and N. G. Greeff. 1992. The early phase of sodium channel gating current in the squid giant axon. Characteristics of a fast component of displacement charge movement. *Eur. Biophys. J.* 21:99–116.

Frehland, E. 1978. Current noise around steady states in discrete transport systems. *Biophys. Chem.* 8:255–265.

Gardiner, C. W. 1990. Handbook of Stochastic Methods for Physics, Chemistry, and the Natural Sciences (corrected edition). Springer-Verlag, Berlin.

Hodgkin, A. L., and A. F. Huxley. 1952. A quantitative description of membrane current and its application to conduction and excitation in nerve. *J. Physiol. (Lond.).* 117:500–544.

Korn, S. J., and R. Horn. 1989. Model selection: reliability and bias (letter to the editor). *Biophys. J.* 55:379–381.

Kramers, H. A. 1940. Brownian motion in a field of force and the diffusion model of chemical reactions. *Physica.* 7:284–304.

Läuger, P. 1988. Internal motions in proteins and gating kinetics of ionic channels. *Biophys. J.* 53:877–884.

Leib, H., and S. Pasupathy. 1992. Digital transmission performance of standard analog filters. *IEEE Trans. Commun.* 40:42–50.

Levitt, D. G. 1989. Continuum model of voltage-dependent gating: macroscopic conductance, gating current, and single-channel behavior. *Biophys. J.* 55:489–498.

Liebovitch, L. S. 1989. Testing fractal and Markov models of ion channel kinetics (letter to the editor). *Biophys. J.* 55:373–377.

Liebovitch, L. S., J. Fischbarg, and J. P. Koniarek. 1987. Ion channel kinetics: a model based on fractal scaling rather than multistate Markov processes. *Math. Biosci.* 84:37–68.

McManus, O. B., C. E. Spivak, A. L. Blatz, D. S. Weiss, and K. L. Magleby. 1989. Fractal models are inadequate for the kinetics of four different ion channels. *Biophys. J.* 54:859–870.

McManus, O. B., D. S. Weiss, C. E. Spivak, A. L. Blatz, and K. L. Magleby. 1988. Fractal models, Markov models, and channel kinetics (letter to the editor). *Biophys. J.* 55:383–385.

Millhauser, G. L., E. E. Salpeter, and R. E. Oswald. 1988. Diffusion models of ion-channel gating and the origin of power-law distributions from single-channel recording. *Proc. Natl. Acad. Sci. USA.* 85: 1503–1507.

Papoulis, A. 1991. Probability, Random Variables, and Stochastic Processes. McGraw-Hill, New York.

Press, W. H., S. A. Teukolsky, W. T. Vetterling, and B. P. Flannery. 1992. Numerical Recipes in C, 2nd Ed. Cambridge University Press, New York.

Rice, S. O. 1944. Mathematical analysis of random noise. *Bell System Tech. J.* 23:282 (reprinted in Wax, N., editor. 1954. Selected Papers on Noise and Stochastic Processes. Dover, New York).

Rumelin, W. 1982. Numerical treatment of stochastic differential equations. *SIAM J. Numerical Anal.* 19:604–613.

Schoppa, N. E., K. McCormack, M. A. Tanouye, and F. J. Sigworth. 1992. The size of gating charge in wild-type and mutant *Shaker* potassium channels. *Science.* 255:1712–1715.

Schoppa, N. E., and F. J. Sigworth. 1998. Activation of *Shaker* potassium channels. III. An activation gating model for wild-type and V2 mutant channels. *J. Gen. Phys.* 111:313–342.

Seoh, S., D. Sigg, D. M. Papazian, and F. Bezanilla. 1996. Voltage-sensing residues in the S2 and S4 segments of the *Shaker* K^+ channel. *Neuron.* 16:1159–1167.

Shapiro, B. E., and H. Qian. 1997. A quantitative analysis of single protein-ligand complex separation with the atomic force microscope. *Biophys. Chem.* 67:211–219.

Sigg, D., and F. Bezanilla. 1997. Total charge movement per channel: the relation between gating charge displacement and the voltage sensitivity of activation. *J. Gen. Physiol.* 109:27–39.

Sigg, D., E. Stefani, and F. Bezanilla. 1994. Gating current noise produced by elementary transitions in *Shaker* potassium channels. *Science.* 264: 578–582.

Sigworth, F. J. 1993. Voltage gating of ion channels. *Q. Rev. Biophys.* 27:1–40.

Starace, D., E. Stefani, and F. Bezanilla. 1997. Voltage-dependent proton transport by the voltage sensor of the *Shaker* K^+ channel. *Neuron.* 19:1319–1327.

Stefani, E., and F. Bezanilla. 1996. Early events in voltage gating. *Biophys. J.* 70:A143 (Abstr.).

Ühlenbeck, G. E., and L. S. Ornstein. 1930. On the theory of the Brownian motion. *Phys. Rev.* 36:823–841 (reprinted in Wax, N., editor. 1954. Selected Papers on Noise and Stochastic Processes. Dover, New York).

Van Kampen, N. G. 1992. Stochastic Processes in Physics and Chemistry. North-Holland Personal Library, Amsterdam.

Zagotta, W. N., T. Hoshi, and R. W. Aldrich. 1994. *Shaker* potassium channel gating. III. Evaluation of kinetic models for activation. *J. Gen. Physiol.* 103:321–362.